Contributions to Mineralogy and Petrology (2021) 176:28
https://doi.org/10.1007/s00410-021-01777-6

ORIGINAL PAPER

Serial interaction of primitive magmas with felsic and mafic crust recorded by gabbroic dikes from the Antarctic extension of the Karoo large igneous province

Jussi S. Heinonen[1,2] · Arto V. Luttinen[3] · Frank J. Spera[4] · Saku K. Vuori[5] · Wendy A. Bohrson[2,6]

Received: 15 September 2020 / Accepted: 3 February 2021

Abstract

Two subvertical gabbroic dikes with widths of ~ 350 m (East-Muren) and ≥ 500 m (West-Muren) crosscut continental flood basalts in the Antarctic extension of the ~ 180 Ma Karoo large igneous province (LIP) in Vestfjella, western Dronning Maud Land. The dikes exhibit unusual geochemical profiles; most significantly, initial (at 180 Ma) ε_{Nd} values increase from the dike interiors towards the hornfelsed wallrock basalts (from − 15.3 to − 7.8 in East-Muren and more gradually from − 9.0 to − 5.5 in West-Muren). In this study, we utilize models of partial melting and energy-constrained assimilation–fractional crystallization in deciphering the magmatic evolution of the dikes and their contact aureoles. The modeling indicates that both gabbroic dikes acquired the distinctly negative ε_{Nd} values recorded by their central parts by varying degrees of assimilation of Archean crust at depth. This first phase of deep contamination was followed by a second event at or close to the emplacement level and is related to the interaction of the magmas with the wallrock basalts. These basalts belong to a distinct Karoo LIP magma type having initial ε_{Nd} from − 2.1 to + 2.5, which provides a stark contrast to the ε_{Nd} composition of the dike parental magmas (− 15.3 for East-Muren, − 9.0 for West-Muren) previously contaminated by Archean crust. For East-Muren, the distal hornfelses represent partially melted wallrock basalts and the proximal contact zones represent hybrids of such residues with differentiated melts from the intrusion; the magmas that were contaminated by the partial melts of the wallrock basalts were likely transported away from the currently exposed parts of the conduit before the magma–wallrock contact was sealed and further assimilation prevented. In contrast, for West-Muren, the assimilation of the wallrock basalt partial melts is recorded by the gradually increasing ε_{Nd} of the presently exposed gabbroic rocks towards the roof contact with the basalts. Our study shows that primitive LIP magmas release enough sensible and latent heat to partially melt and potentially assimilate wallrocks in multiple stages. This type of multi-stage assimilation is difficult to detect in general, especially if the associated wallrocks show broad compositional similarity with the intruding magmas. Notably, trace element and isotopic heterogeneity in LIP magmas can be homogenized by such processes (basaltic cannibalism). If similar processes work at larger scales, they may affect the geochemical evolution of the crust and influence the generation of, for example, massif-type anorthosites and "ghost plagioclase" geochemical signature.

Keywords Large igneous provinces · Magmatism · Differentiation · Assimilation · Modeling

Introduction

Large igneous provinces (LIPs) are remnants of unusually voluminous intraplate magmatic events with estimates of total magmatic volumes of > 0.1 Mkm^3 (up to 10 Mkm^3; White and McKenzie 1989) emplaced during a few million years (Bryan and Ernst 2008). Such events are known to have taken place sporadically throughout Earth history (e.g., Ernst 2007). Even though Phanerozoic continental mafic LIPs are usually associated with thick sequences of widespread continental flood basalts (CFBs), most of their igneous volume is expected to be hidden within the lithosphere (e.g., Cox 1980; White and McKenzie 1989; Coffin and Eldholm 1994; Ernst et al. 2019). Indeed, many Precambrian LIPs that have lost most of their supracrustal parts due to tectonism, weathering, and erosion have been recognized based on outcrops of

Communicated by Mark S Ghiorso.

✉ Jussi S. Heinonen
jussi.s.heinonen@helsinki.fi

Extended author information available on the last page of the article

Published online: 30 March 2021

extensive dike swarms and other mafic–ultramafic intrusive rocks that are temporally related (e.g., LeCheminant and Heaman 1989; Wingate et al. 2004). Since basalts are relatively easily weathered and eroded, intrusive rocks are also exposed in many younger mafic LIPs (e.g., Vanderkluysen et al. 2011; Luttinen et al. 2015).

When emplaced within the lithosphere, LIP magmas have tended to thermally and chemically react with their surroundings. This is evidenced by field observations of wallrock partial melting near intrusions (e.g., Johnson et al. 2003; Hersum et al. 2007) as well as geochemical evidence of assimilation having modified the compositions of the erupted lavas (e.g., Brandon et al. 1993; Baker et al. 1996; Hansen and Nielsen 1999). Such interactions are likely to be concentrated in magma chambers and conduits within intermediate to deep (≥ 10 km) crust, where the residence times are longer and the wallrock is warmer, compared to shallower systems (e.g., Tegner et al. 2005; Heinonen et al. 2019). Nevertheless, evidence of assimilation has also been observed or indicated for some shallower feeder systems (e.g., Lightfoot and Naldrett 1989; Neumann et al. 2011; Yallup et al. 2013; Hayes et al. 2015). Overall, as the magmas travel through a lithologically and geochemically heterogeneous lithosphere, multiple stages of contamination may take place (see, e.g., Neumann et al. 2011). These are not always easily distinguishable from each other when analyzing the final crystallization products.

In this study, we present additional geochemical and Nd isotopic whole-rock data for selected samples from two previously described gabbroic dikes related to the Antarctic portion of the ~ 180 Ma Karoo LIP (Fig. 1). The gabbroic dikes are ~ 350 and ≥ 500 m wide and crosscut Karoo CFBs in East- and West-Muren nunataks, respectively, in Vestfjella, western Dronning Maud Land. We demonstrate that the dikes record two stages of interaction between the parental magmas and wallrock: first with Archean tonalite–trondhjemite–granodiorite (TTG) wallrocks at middle to lower crustal depths and then with the flood basalt wallrocks at

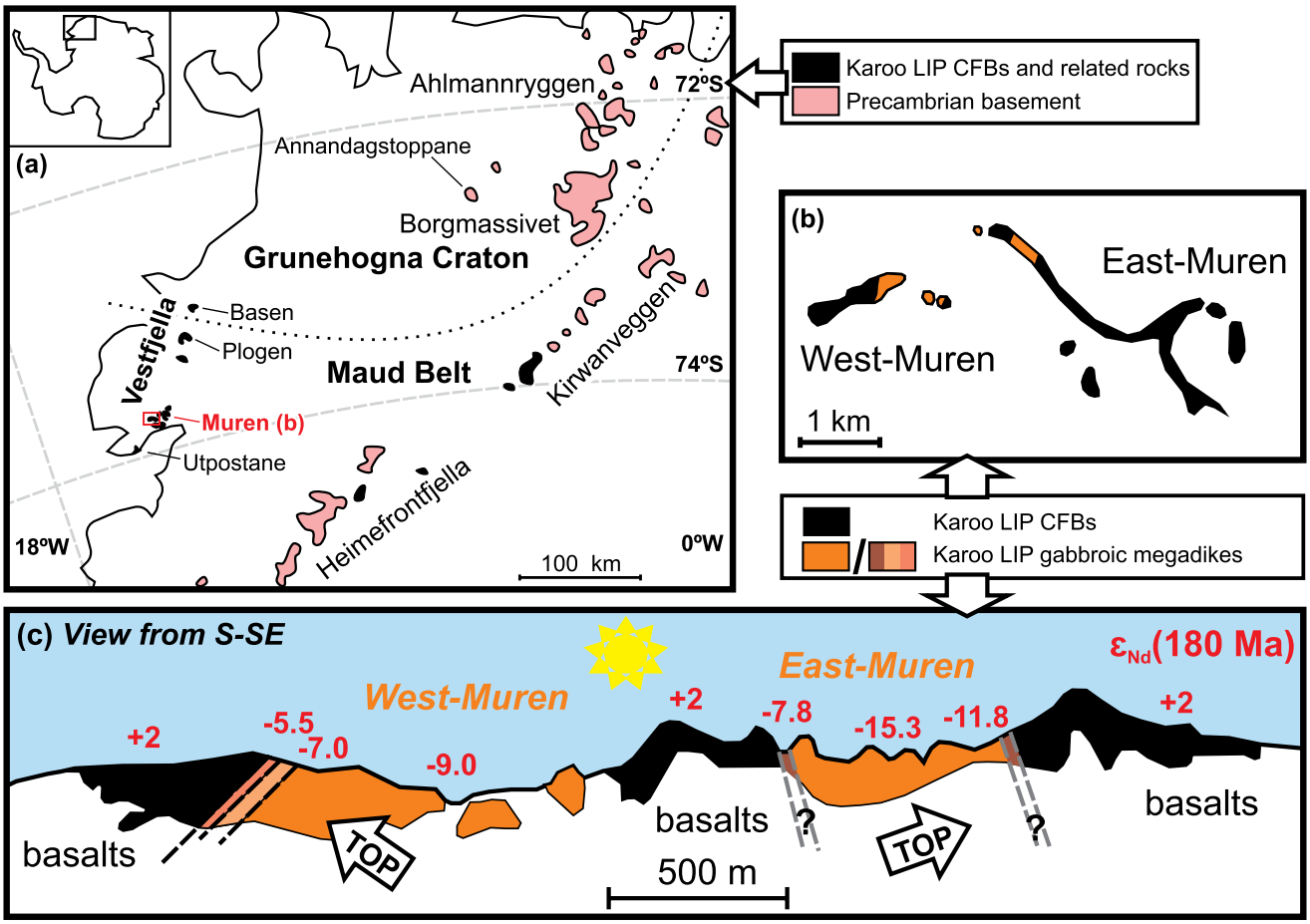

Fig. 1 **a** Distribution of Jurassic Karoo LIP CFBs and related rocks in western Dronning Maud Land, Antarctica. Lithospheric boundary reconstructed after Corner (1994). **b** Muren nunataks (note location in a). **c** Schematic horizontal view of the Muren gabbroic dike outcrops from SSE towards NNW. The dip of the East-Muren gabbroic dike is not very precisely known. The top arrows refer to the orientations of the cross-sections illustrated in Figs. 3 and 4

or close to the present exposure level. Given that the flood basalt wallrocks have mantle-derived geochemical signatures, the most contaminated outer zones of the gabbroic dikes show higher initial (at 180 Ma) ε_{Nd} values than the inner parts that only record assimilation of TTGs. This study presents evidence of a two-stage CFB magmatic contamination scenario that would not be easily traceable without data from the intrusive rocks. It, thus, highlights the importance of studying intrusive members of CFB provinces and has broader relevance to research on the evolution of magmatic systems and the crust in general.

Geological setting

Regional geology

The bedrock of western Dronning Maud Land contains rocks spanning in age from Archean to Jurassic. The Archean Grunehogna craton is only exposed in Annandagstoppane (Marschall et al. 2010), but is likely to constitute most of the northwestern parts of the area based on geophysical data (Corner 1994) (Fig. 1a). The Grunehogna craton was separated from the associated Kaapvaal craton of southern Africa during Gondwana breakup (e.g., Jacobs et al. 2008). In the Ahlmannryggen and Borgmassivet areas, the Grunehogna craton is overlain by metamorphosed and deformed supracrustal rocks belonging to the ~ 1100 Ma Proterozoic Ritscherflya Supergroup (Wolmarans and Kent 1982; Moyes et al. 1995) and contemporary or slightly younger Borgmassivet intrusions that are likely related to the Umkondo LIP of southern Africa (e.g., Riley and Millar 2014) (Fig. 1a). The Grunehogna craton is fringed to the south and east by highly complex, deformed, and metamorphosed Proterozoic supracrustal belts that have experienced several stages of thermal and tectonic reworking (e.g., Jacobs et al. 2003, 2015; Grosch et al. 2007, 2015; Romu 2019). Overlying the Precambrian basement are Paleozoic fossil-bearing sedimentary rocks (e.g., McLoughlin et al. 2005) and the Karoo LIP CFBs and associated intrusive rocks (see below), which are geochemically distinct from contemporaneous Ferrar LIP CFBs that are more widespread in Antarctica.

Vestfjella flood basalts

The CFBs and related intrusive rocks of Vestfjella exhibit considerable geochemical heterogeneity with, e.g., initial ε_{Nd} ranging from − 17 to + 8 (Fig. 2b; Luttinen et al. 2015). The Vestfjella CFBs can be divided into four fairly distinct types (Luttinen and Furnes 2000), of which two volumetrically dominant ones are important for this study (Fig. 2): (A) low-ε_{Nd} CT1 lavas exhibit low Ti/Zr (30−70), Ti/P (6−13), but have high Th/Ta (3–7) and very low initial ε_{Nd} from − 16 to − 11; (B) CT3 lavas have high Ti/Zr (80–180), low Ti/P (7–14) and Th/Ta (1–3), and initial ε_{Nd} from − 2 to + 2. Both magma types may have been derived from similar kinds of primary magmas that themselves were derived from variably subduction-modified depleted upper mantle (Luttinen

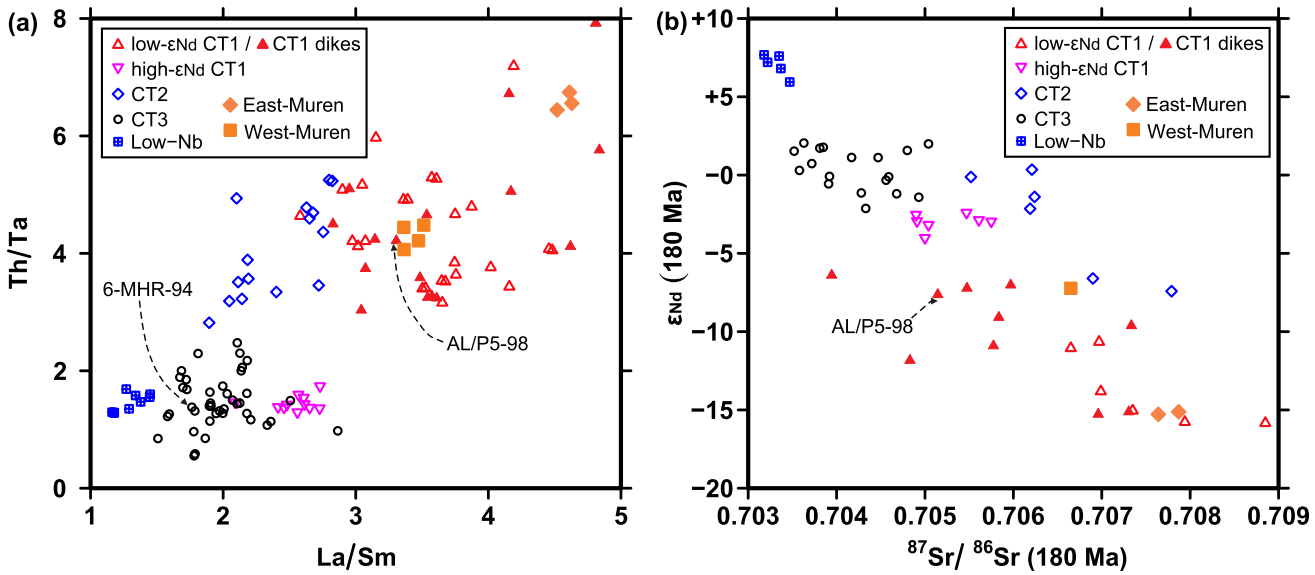

Fig. 2 Geochemical heterogeneity of the Vestfjella CFBs (including CT1 dikes) shown in La/Sm vs. Th/Ta (**a**) and initial $^{87}Sr/^{86}Sr$ vs. intial ε_{Nd} (**b**) diagrams. Samples from EM middle zone and WM main zone (see Figs. 3, 4) are shown for reference. CT1 dike sample AL/P5-98 and CT3 sample 6-MHR-94 discussed in the text are highlighted (the latter only in **a**, because of lack of Sr isotopic data). Data sources in addition to this study: (Luttinen and Siivola 1997; Luttinen et al. 1998, 2015; Luttinen and Furnes 2000; Vuori and Luttinen 2003; Luttinen and Vuori 2006; Heinonen et al. 2010)

and Furnes 2000; Heinonen et al. 2016, 2018; Luttinen, 2018) This asthenospheric mantle source has also been sampled by primitive and isotopically depleted dikes found in the area (Low-Nb magma type of Heinonen et al. 2010). Previous geochemical modeling suggests that the low-ε_{Nd} CT1 lavas assimilated < 20% of Archean crust (relative to the initial mass of the parental melt; Heinonen et al. 2016, 2019), whereas the CT3 lavas do not show evidence of crustal contamination, but probably incorporated materials from the enriched parts of the subcontinental lithospheric mantle (Heinonen et al. 2016).

East- and West-Muren gabbroic dikes

In addition to a mafic layered intrusion at Utpostane and a wide variety of dikes (including lamproites and ferropicrites; for an overview, see Luttinen et al. 2015) with widths commonly less than 10 m, Vestfjella hosts two exceptionally large dike-like and coarse-grained mafic intrusions crosscutting CT3-type basalts at East-Muren (hereafter EM gabbroic dike) and West-Muren (hereafter WM gabbroic dike) (Fig. 1). These dikes were first mapped as belonging to a single mafic intrusion entraining a 300-m-wide basaltic megaxenolith (Vuori and Luttinen 2003), but later observations and geochemical differences revealed them to be two separate and geochemically distinct intrusions having widths of ~ 350 (EM) and at least ~ 500 (WM) meters (Vuori 2004; Luttinen et al. 2015). Their lengths along strike are unknown, but as their orientations conform to the dominant strike direction (~ NNE–SSW) of a plethora of smaller dikes in the area, it is assumed that they represent at least somewhat tabular intrusions. The first lithological and geochemical profiles and outcrop and thin section photographs were provided by Vuori and Luttinen (2003). More detailed profiles (now separating the two intrusions), trace element data, and thin section photographs are illustrated in Figs. 3, 4, 5, and 6.

The EM gabbroic dike has an approximately NNE–SSW strike that corresponds to that of the majority of the other smaller dikes in the area. Its dip has not been precisely defined because of limited exposure, but it is probably vertical or subvertical towards ESE (Fig. 1c). Its inner parts (middle zone) are characterized by rather homogeneous, medium-grained, intergranular, and olivine-poor (< 1 – 4 vol.%) leucogabbronorites and gabbronorites showing uniform whole-rock compositions (e.g., MgO ≈ 6–8 wt.%).

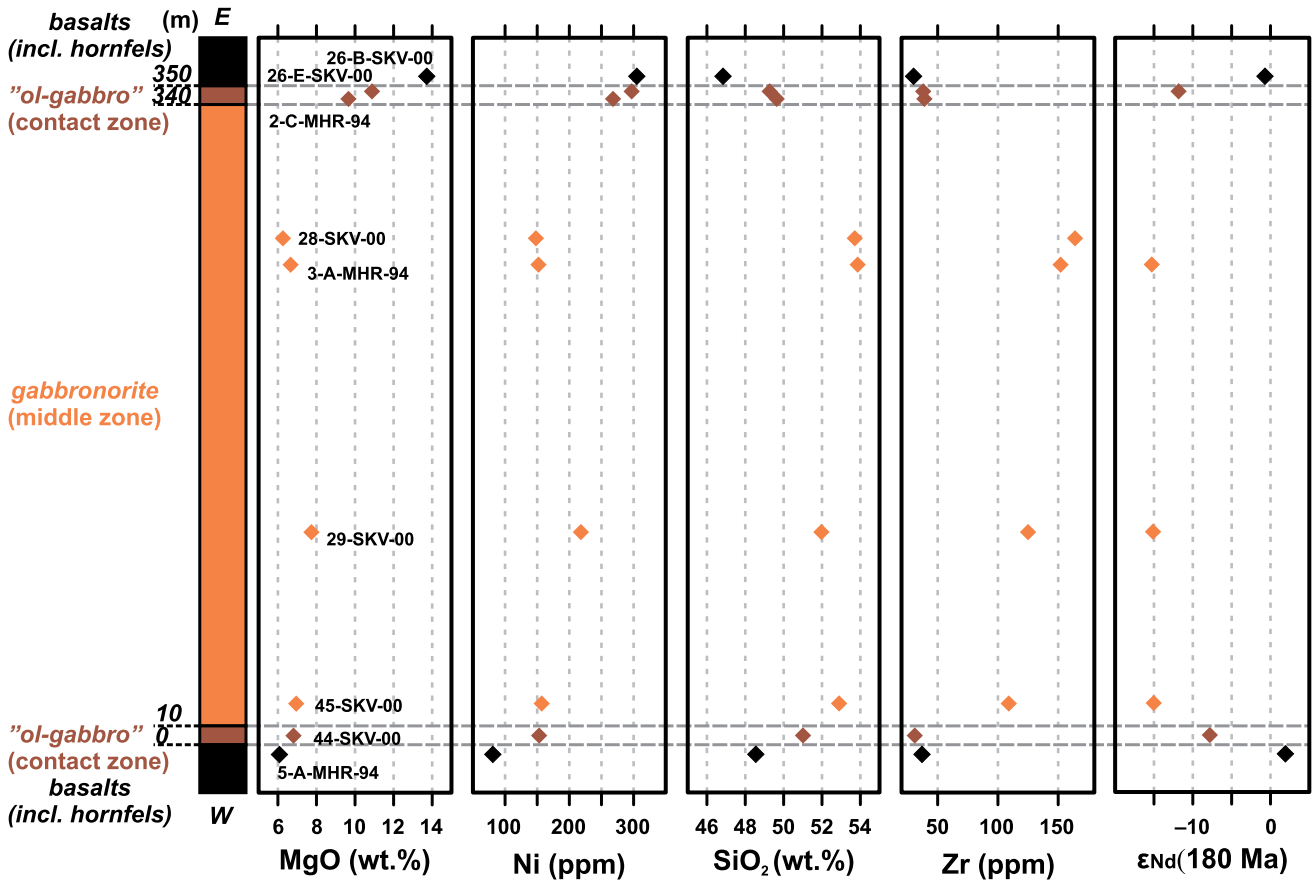

Fig. 3 Geochemical and simplified rock type profile across the East-Muren gabbroic dike

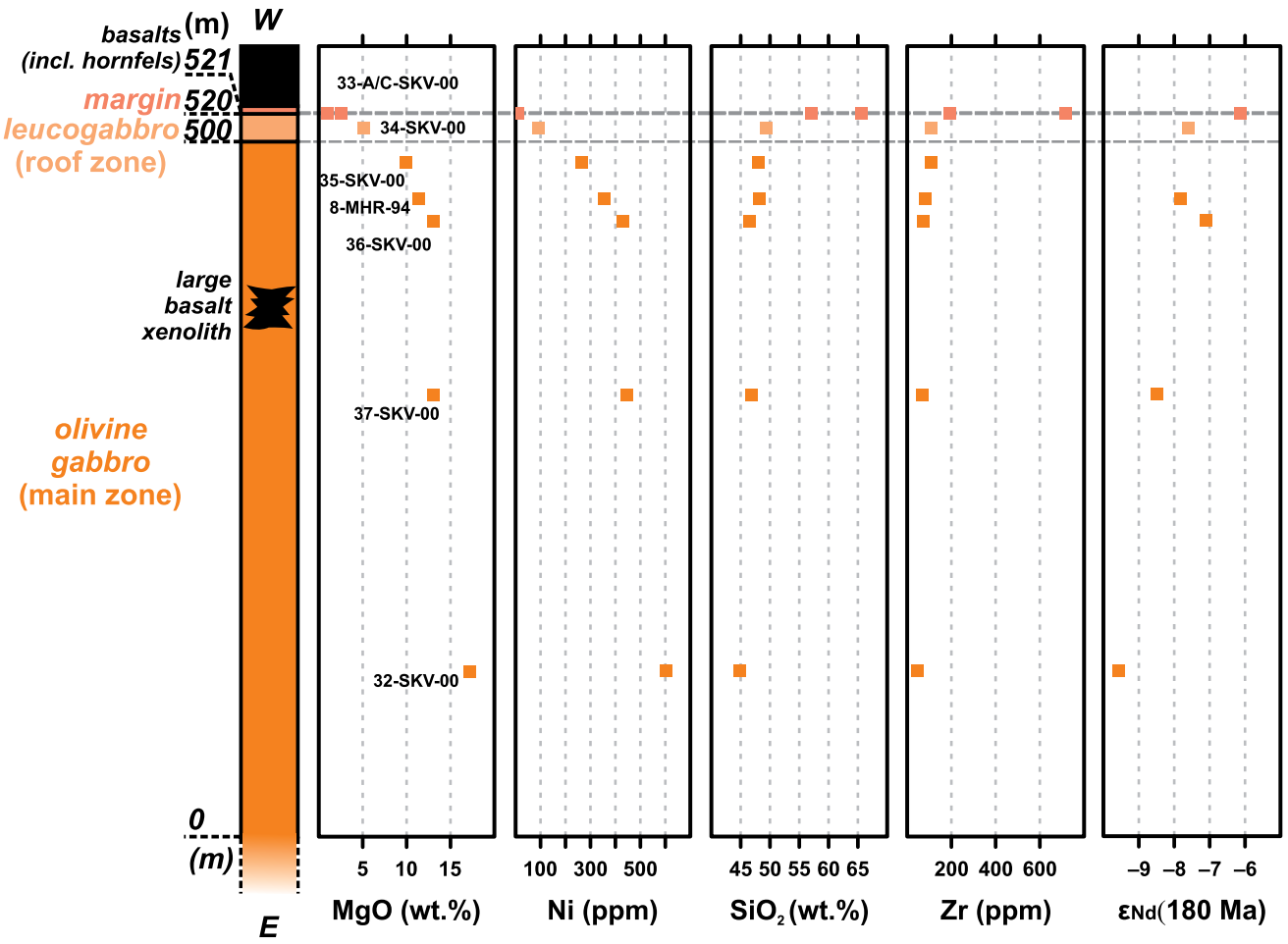

Fig. 4 Geochemical and simplified rock type profile across the West-Muren gabbroic dike

There are no indications of magmatic layering, but distinctive narrow (~ 10 m) contact zones can be distinguished on both sides (Figs. 3 and 6a, b). These zones are characterized by medium-grained rocks that have been classified as olivine gabbros on the basis of their modal compositions (10–15 vol.% of olivine; Fig. 6b). They do not show cumulus textures and contain pyroxene-rich stripes and leucocratic intercalations. The olivine in the rocks exhibits poikilitic texture (Fig. 6b). Compositionally, the olivine gabbro of the eastern contact zone is considerably more magnesian (MgO ≈ 10–11 wt.%) than that of the western contact zone (~ 7 wt.%). Wallrock basalts have been variably metamorphosed into hornfels on both sides (Fig. 6c). The hornfelses are very heterogeneous in appearance, but often show relict porphyritic texture (Fig. 6c). An offshoot dike 400 m away from the contact across strike (sample 31-SKV-00; not part of the stratigraphy in this study) has been associated with the intrusion.

The WM gabbroic dike also strikes approximately NNE–SSW but dips towards WNW (~ 50°) (Fig. 1c). Its inner parts (main zone) have a uniform field appearance and consist of medium-grained olivine gabbros that show gradual enrichment in MgO (from 10 to 17 wt.%) and modal olivine (from 16 to 33 vol.%) towards the eastern basal contact (Figs. 4 and 6d). Clinopyroxene exhibits poikilitic texture (Fig. 6d). Occasional strongly contact metamorphosed basaltic xenoliths are found within the WM intrusion; an exceptionally large one is exposed between the middle zone samples 36-SKV-00 and 37-SKV-00 (Fig. 4). The basal contact is not exposed. One tiny gabbroic outcrop (sample 38-SKV-00; Vuori and Luttinen (2003)) is found at a distance of 1 km following the strike of the main body, but since the relationship of this outcrop to the main body is unknown, we do not consider it part of the stratigraphy in this study. The western top contact is well exposed at one locality and includes a ~ 20-m-thick roof zone composed of coarse-grained and strongly altered leucogabbro with abundant plagioclase. Immediately above that and in contact with the hornfelsed basalts is a ~ 1-m-thick marginal intermediate–felsic unit that consists of heterogeneous, medium-grained, and hypidiomorphic quartz-diorite or tonalite

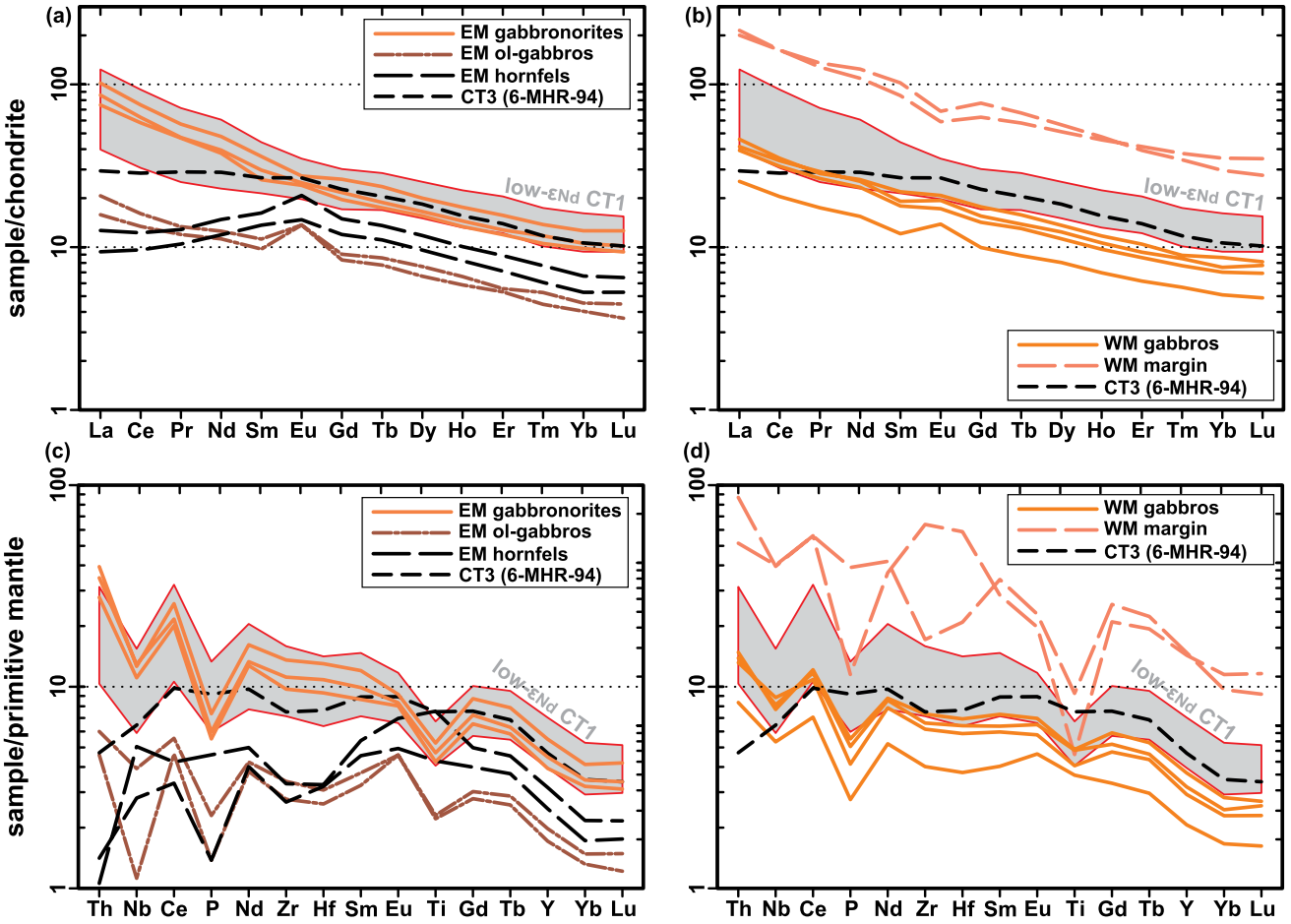

Fig. 5 Rare earth element (**a**, **b**) and incompatible trace element (**c**, **d**) patterns of the Muren gabbroic dikes, low-ε_{Nd} CT1 CFBs, and wallrock CT3 basalt. Note that there is no ICP-MS data available for the WM roof zone sample 34-SKV-00. Normalization values for chondrite from McDonough and Sun (1995) and for primitive mantle from Sun and McDonough (1989). Data sources in addition to this study: Luttinen and Siivola (1997), Luttinen et al. (1998), Luttinen and Furnes (2000), Vuori and Luttinen (2003), and Luttinen and Vuori (2006)

(MgO ≈ 1–3 wt.%, SiO_2 ≈ 57–66 wt.%; Fig. 6e, f). It is commonly altered and contains varying amounts of dendritic amphibole that is most common close to the contact with the wallrock basalt and adjacent to the sporadic basalt xenoliths. Again, the wallrock basalts there appear to be contact metamorphosed.

On the basis of their trace element and Sr and Nd isotopic compositions (low Ti/Zr, Ti/P, and initial ε_{Nd}; high La/Sm, Sm/Yb, Th/Ta, and initial $^{87}Sr/^{86}Sr$; Figs. 2 and 5), both gabbroic dikes have been suggested to be petrogenetically linked to the CT1 lavas (Luttinen and Vuori 2006; Luttinen et al. 2015). The wallrock basalts belong to the CT3 magma type (Fig. 2).

Samples and analytical methods

Most of the data utilized in this study have been previously published in Vuori and Luttinen (2003), Luttinen and Vuori (2006), and Luttinen et al. (2015). To acquire a more detailed view of the geochemical variation and differentiation processes of the magmas, we performed additional major and trace element and Nd isotopic analyses on selected samples from the gabbroic dikes and their wallrock basalts. All geochemical data are tabulated in the online Online Resource 1.

Major and trace elements

Major elements and some trace elements (Cr, Ni, Sc, V, Cu, Zn, Ga, Nb, Zr, Ba, and Sr reported) were analyzed with X-ray fluorescence (XRF) for an olivine gabbro from the EM basalt contact zone (sample 44-SKV-00) and for an unmelted wallrock basalt collected ~ 250 m away from

the contact (6-MHR-94) at the Peter Hooper Geoanalytical Laboratory, Washington State University. Fresh chips were picked for the analysis after crushing hand-sized samples in a steel jaw crusher. A tungsten carbide mill was used for preparation of powders. Technical notes of the method are given by Johnson et al. (1999). Major element data are discussed and plotted normalized to 100 wt.% volatile-free in this study.

Leucogabbronorite from the EM middle zone (45-SKV-00) and samples 44-SKV-00 and 6-MHR-94 (see above), and three olivine gabbros from the WM main zone (32-SKV-00, 36-SKV-00, and 37-SKV-00) were also analyzed for rare-earth elements (REE) and other incompatible trace elements (Ta, Hf, Y, Rb, U, Th, and Pb reported) using inductively coupled plasma mass spectrometry (ICP-MS) at the same facility. For this analysis, the hand-picked chips were powdered in an iron bowl in a shatter-box swing mill. Technical notes of the method are given by Knaack et al. (1994).

Examples of repeated analyses of basaltic standards using both methods are reported in Luttinen et al. (2015) and Turunen et al. (2019). The precision is generally very good for major elements (< 2% relative) and trace elements (< 5% relative) that are found in relatively high concentrations in the standard materials. In addition, the reported analyses for the standard materials show deviations of less than 5% from the recommended values. Only Pb analyzed with ICP-MS shows consistently large deviations (10–40%) from the standard materials.

Nd isotopes

Neodymium isotopic compositions of a contact zone olivine gabbro (44-SKV-00), a middle zone leucogabbronorite (45-SKV-00), and two basalt hornfels samples (26-B-SKV-00 and 5-A-MHR-94) from EM, three main zone olivine gabbros (32-SKV-00, 36-SKV-00, and 37-SKV-00) from WM, and an unmelted wallrock basalt (6-MHR-94) were analyzed using Thermo Scientific Triton TIMS at the Isotope Geochemistry Laboratories of the Department of Geological Sciences, University of Texas at Austin (Online Resource 1). The analyses were performed using the same powders that were previously prepared for the major and trace element analyses.

For the Nd isotopic analyses, 50–100 mg of powder were dissolved in 49 N HF and 15 N HNO_3 (4:1) on a hot plate at 150 °C for 4 days. Samples were then dried and redissolved in 15 N HNO_3 overnight in the same temperature. Any precipitates were broken down by adding 12 N HCl. Samples were dried again and redissolved in 15 N HNO_3 to eliminate chlorides, then dried and dissolved in 2 N HNO_3. REE were isolated in 200 µl columns using RE-SPEC resin, then dried and dissolved twice (first in 6 N HCl and then 0.3 N HCl) to isolate Nd. Final isolation of Nd took place in prefilled calibrated columns using LN-SPEC resin. Samples were then loaded on Re filaments in dilute H_3PO_4.

The measurement of full procedural blank yielded 15 pg Nd, which is insignificant relative to the 250–1000 ng Nd in the samples. The Nd isotopic ratios were corrected for fractionation using $^{146}Nd/^{144}Nd$ of 0.7219 and an exponential fractionation law. Repeated analysis of an in-house AMES Nd standard gave $^{143}Nd/^{144}Nd$ of 0.512087 ± 0.000010 (2σ). This is in agreement with the recommended value of 0.512088 ± 0.000176 (2σ) based on 76 repeated analyses in other labs as reported by the utilized lab. ICP-MS Nd and Sm data were used to calculate $^{147}Sm/^{144}Nd$ and back-calculate ε_{Nd} at 180 Ma (initial ε_{Nd}).

Results

Since most of the data discussed in this study has previously been published (Vuori and Luttinen 2003; Luttinen et al. 2015; see Online Resource 1), all the new data have been appended in Figs. 2, 3, 4, and 5 and only a short summary of the results is given here. The new data confirm the previously presented view that the main zones of both gabbroic dikes show general geochemical affinity to the low-ε_{Nd} CT1 basalts (Figs. 2 and 5).

The EM middle zone gabbronorites exhibit rather uniform compositions in terms of major element, trace element, and especially Nd isotopic compositions ($\varepsilon_{Nd} = -15$) (Figs. 3 and 5). The contact zone olivine gabbros exhibit compositions (for example, in terms of MgO, SiO_2, Ni, and Nd isotopes) that plot between the gabbronorites and the contact metamorphosed wallrock basalts that vary in composition on different sides of the gabbroic dike (Fig. 3). On the other hand, the olivine gabbros show lower HREE contents than the basalt hornfelses while manifesting a relative LREE enrichment similar to that of the middle zone gabbronorites (Fig. 5a). The olivine gabbros also show a positive Eu anomaly that is missing from the gabbronorites. The REE patterns of the basalt hornfelses are reminiscent of that of the more pristine CT3 basalt, although they show a positive Eu anomaly and are more depleted in LREE. The incompatible element patterns of the contact zone olivine gabbros resemble those of the middle zone gabbronorites, but are much more depleted and variable, especially in terms of highly incompatible elements (Fig. 5c). Similar to the pristine CT3 basalt, the basalt hornfelses have concave incompatible trace element patterns, but the element ratios are quite variable and the concentrations are relatively low.

The WM main zone olivine gabbros show general increase in SiO_2, incompatible trace elements, and initial ε_{Nd} (from −9 to −7), and decrease in MgO and compatible trace elements from the base towards the upper contact (Fig. 4). The intermediate–felsic margin shows

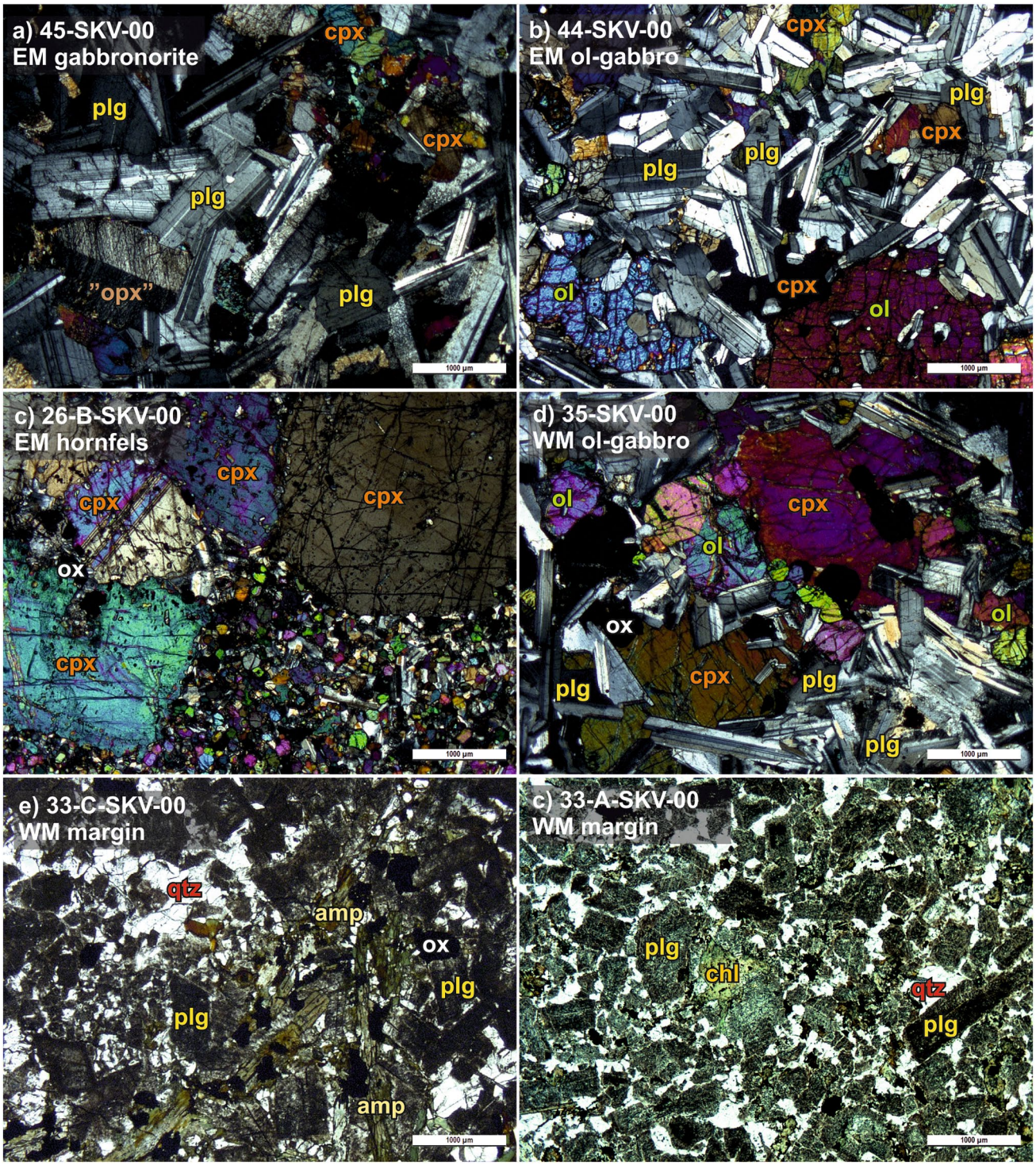

considerable variation in composition depending on whether the sample comes from more amphibole-rich parts close to the contact with the wallrock basalts (sample 33-C-SKV-00) or closer to the main zone (sample 33-A-SKV-00). The concentrations of incompatible trace elements in the main zone are lower than in the low-ε_{Nd} CT1 basalts on average and the negative Nb, P, and Ti anomalies are less pronounced (Fig. 5). The intermediate–felsic margin of the dike shows internal variation in incompatible trace element pattern, especially in terms of P, Zr, and Hf (Fig. 5d): the amphibole-rich sample 33-C-SKV-00 exhibits notable relative Zr and Hf depletion, whereas the more felsic sample 33-A-SKV-00 that

◂**Fig. 6** Thin section photographs of the Muren gabbroic dikes (**a–d** in cross-polarized light, **e–f** in plane-polarized light). **a** Gabbronorite (SiO_2 = 53 wt.%, MgO = 7 wt.%) from the middle zone of EM gabbroic dike. Note the thin herringbone clinopyroxene exsolution lamellae in the orthopyroxene crystal, suggesting that it represents inverted pigeonite. **b** "Olivine gabbro" (SiO_2 = 51 wt.%, MgO = 7 wt.%) from the lower contact zone of EM gabbroic dike. Note the spongy olivine and clinopyroxene with plagioclase inclusions and plagioclase with rounded corners. **c** Basalt hornfels (SiO_2 = 47 wt.%, MgO = 14 wt.%) from the upper contact of the EM gabbroic dike. Note the resorbed and inclusion-rich clinopyroxene phenocrysts. The groundmass is composed of olivine, plagioclase, Fe–Ti oxides and minor clinopyroxene. **d** Olivine gabbro (SiO_2 = 48 wt.%, MgO = 10 wt.%) from the main zone of the WM gabbroic dike. **e** Quartz diorite (SiO_2 = 57 wt.%, MgO = 3 wt.%) from the intermediate–felsic margin of the WM gabbroic dike. Note the abundant acicular amphibole and saussuritization of plagioclase. **f** Tonalite (SiO_2 = 66 wt.%, MgO = 1 wt.%) from the intermediate–felsic margin of the WM gabbroic dike. Note the saussuritization of plagioclase and secondary chlorite. *Ol* olivine, *opx* orthopyroxene, *cpx* clinopyroxene, *amp* amphibole, *plg* plagioclase, *ox* Fe-Ti oxides, *chl* chlorite. Scale bar width is 1 mm in all photographs

contains relatively higher amount of accessory zircon exhibits Zr and Hf enrichment and relative P depletion.

Discussion

Judging from geochemical similarity, the Muren gabbroic dikes are intrusive equivalents of the low-ε_{Nd} CT1 basalts (Luttinen and Vuori 2006; Luttinen et al. 2015). Recent modeling of the differentiation of the basalts suggested a two-stage process: assimilation of ≤ 15% of Archean crust at depths of ~ 10–30 km followed by fractional crystallization at shallower levels without significant additional assimilation (Heinonen et al. 2016, 2019). We argue that the petrogenesis of the Muren gabbroic dikes involved these two stages with the addition that some shallow assimilation also took place. These stages are discussed in intrusion-specific sections below and, subsequently, we address the regional and global implications of our results.

Deep assimilation of Archean crust

Modeling of the assimilation of Archean crust by the low-ε_{Nd} CT1 magmas is mostly hampered by uncertainties in the geochemical composition of the primary mantle-derived melt, especially in terms of major elements (see Heinonen et al. 2019), whereas the variability of Archean crustal compositions is reasonably constrained by sampling at the level of exposure in Africa (see, e.g., Kreissig et al. 2000). To model the assimilation of the Archean TTGs by the EM and WM magmas, we utilize the energy-constrained assimilation−fractional crystallization (EC-AFC) equations of Spera and Bohrson (2001). These equations do not require exact knowledge on the major element composition of the parental melt, which is unknown and very difficult to constrain. The incompatible trace element and Nd isotopic composition of the parental melt, however, has been estimated on the basis of estimations on the degree of melting and the geochemistry of the depleted low-Nb dikes (see Heinonen et al. 2016). A spatially associated Archean TTG (Kreissig et al. 2000; sample 96/203 with isotopic variation observed in TTGs in the region) is used as an assimilant. The full background and parametrization of this model is presented in Heinonen et al. (2016) with the following exception: instead of using a constant wallrock/melt bulk partition coefficient of 0.1 or 0.5 for every element, the bulk partition coefficients were set to vary linearly from 0.1 for Th to 0.5 for Lu. These values are compatible with listings of partition coefficients relevant for felsic crustal rocks and their phases (see, e.g., https://earthref.org/KDD/) and approximate the relative incompatibility of the modeled elements when the mineral composition of the assimilant has not been reported (Kreissig et al. 2000) and is neither modeled in EC-AFC. We used the gabbroic dike samples with the strongest affinities to Archean crust for the comparisons (see the following sections). In the case of EM, these are the middle zone gabbronorites, and for the WM, the main zone olivine gabbros. The best-fit models are illustrated in Fig. 7.

Assimilation of Archean crust recorded by the East-Muren gabbroic dike

The best-fit EC-AFC model for the EM gabbronorites suggests 6% of assimilation of Archean TTG anatectic melt relative to the mass of the parental melt (Fig. 7a). The major differences between the modeled and observed compositions are the relatively lower Nb, Zr, Hf, Sm, and Eu and higher Ti in the model. We consider that the model reproduces the characteristic incompatible patterns and ε_{Nd} values (from − 19 to − 12 in the model vs. − 15 in the samples) of the EM gabbroic dikes reasonably well (Fig. 7a).

Assimilation of Archean crust recorded by the West-Muren gabbroic dike

The best-fit EC-AFC model for the WM olivine gabbros indicates 3% of assimilation relative to the mass of the parental melt (Fig. 7b), which is half of the relative amount of assimilation suggested for the EM middle zone gabbronorites. The major differences between the modeled and observed compositions are the relatively lower Nb and marginally higher Ti and heavy REE contents in the model. Again, these are considered as minor discrepancies and the model shows good fit in general also in terms of initial ε_{Nd}

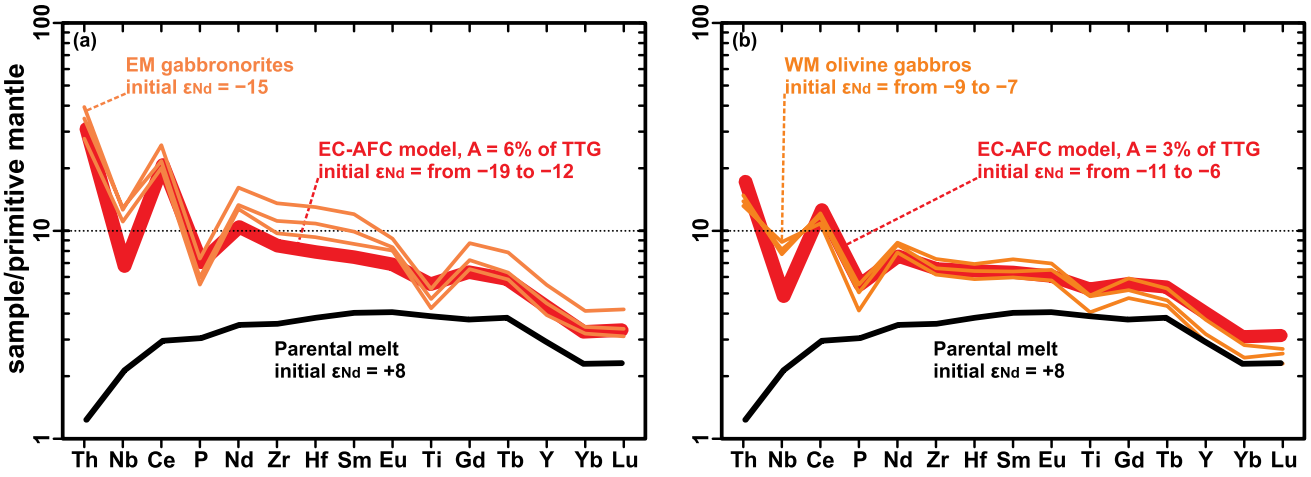

Fig. 7 Best-fit EC-AFC model results for the EM (**a**) and WM (**b**) gabbroic dikes shown in incompatible trace element diagrams normalized to primitive mantle of Sun and McDonough (1989). Percentages indicate the mass of the assimilated material relative to the mass of the original melt. Parental melt composition also shown. See section "Deep assimilation of Archean crust" for more details

(from − 11 to − 6 in the model, from − 9 to − 7 in the samples; Fig. 7b).

Subsequent shallow assimilation of CT3 flood basalts

In this section, we examine the interactions of the EM and WM magmas with the surrounding CT3 flood basalts at or close to the present level of exposure. Such interactions are indicated, e.g., by the geochemical profiles in the gabbroic dikes and the wallrock basalts (Figs. 3 and 4).

Interaction with basalt recorded by the East-Muren gabbroic dike

The thin contact zones of the EM gabbroic dike are composed of olivine gabbros with initial ε_{Nd} from − 12 to − 8 and the middle zone is composed of more evolved gabbronorite with initial ε_{Nd} of − 15 (Fig. 3). A straightforward explanation for this geochemical variation would be that the contact zones represent an early pulse of magma that was less contaminated by Archean crust in the deep open system, whereas the middle zone crystallized from subsequent intrusion(s) of more strongly contaminated magma. Three observations render such scenario unlikely, however:

(1) The olivine gabbros in the contact zones do not show chilled margins or cumulate textures, but are instead characterized by leucocratic intercalations (Vuori and Luttinen 2003), spongy and anhedral olivine with inclusions, and plagioclase with curved grain boundaries (Fig. 6b). These features indicate the potential involvement of disequilibrium, partial melting, hybridization, and/or recrystallization processes. In comparison, the middle zone gabbronorite has a rather pristine igneous texture (Fig. 6a).

(2) Despite not showing cumulate textures, the contact zone olivine gabbros show very low incompatible trace element concentrations (Fig. 5a, c), which could suggest the involvement of partial melting processes.

(3) The Ni and Mg concentrations of the contact zones plot between the middle zone and the wallrock basalt hornfelses; this transitional nature of the contact zones is especially noteworthy given that the MgO and Ni of the hornfelses are different (e.g., lower for the basal wallrock and higher for the upper contact; Fig. 3). Similar transitional correlations can also be observed in terms of most other major and trace elements and Nd isotopes (Fig. 3). This suggests that the contact zone olivine gabbros are petrogenetically linked to the adjacent hornfelses—and, thus, the wallrock basalts—on both sides.

To trace the origin of the EM contact zones and the associated basalt hornfelses in more detail, we tested a hypothesis of partial melting of wallrock basalt (for the hornfelses; Fig. 8) and partial melting of wallrock basalt followed by hybridization of the solid residue with infiltrating EM magma (for the contact zones; Fig. 9). In the modeling, we concentrated on REE (including Nd isotopes) that show coherent behavior in igneous processes in general. Local CT3 basalt sample 6-MHR-94 was used to represent the pristine wallrock REE composition (Fig. 5) and, since the CT3 basalts show flow-by-flow isotopic variation that has not been tracked all around the intrusion, the Nd isotopic composition of the wallrock basalt was chosen to represent the range shown by the CT3 magma type (initial ε_{Nd} = from − 2.1 to + 2.5). The modal composition of the

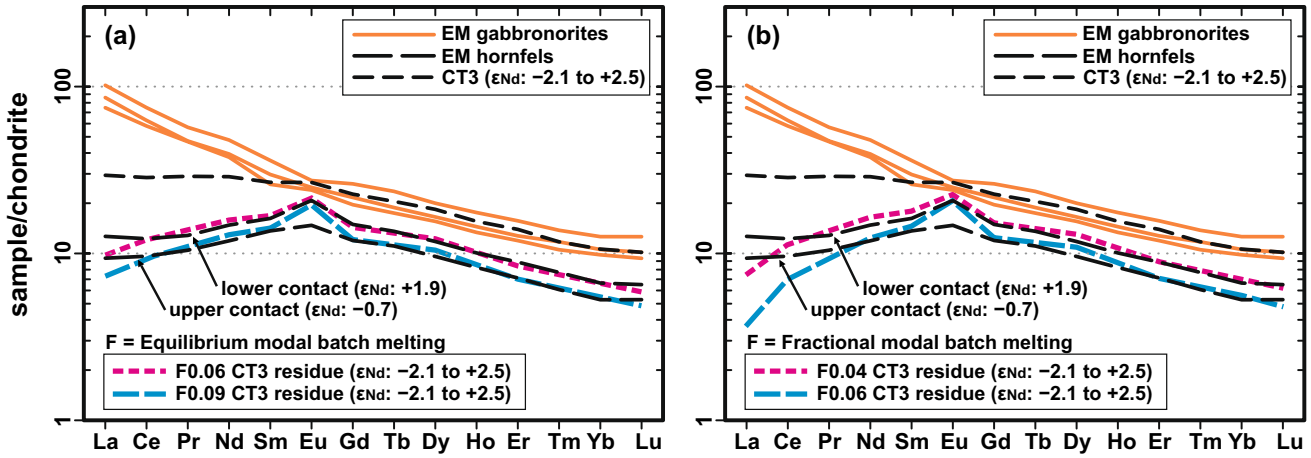

Fig. 8 Results of modeling of equilibrium batch melting (**a**) and fractional batch melting (**b**) of CT3 wallrock basalt (sample 6-MHR-94 with Nd isotopic variation of CT3 basalts) to simulate the formation of the EM hornfelses shown in REE diagrams normalized to chondrite of McDonough and Sun (1995). Partition coefficients for a wallrock basalt mode of 20% olivine, 30% clinopyroxene, and 50% plagioclase were those reported by Schnetzler and Philpotts (1970) (sample HHP-66–19 for olivine, sample GSFC193 for clinopyroxene, and sample GSFC208 for plagioclase) for Ce, Nd, Sm, Eu, Gd, Dy, Yb, and Lu (Lu only reported for plagioclase). Partition coefficients for La and Lu for olivine and clinopyroxene were approximated by polynomial extrapolation (without Eu). "F" denotes the degree of partial melting (equilibrium in **a** and fractional in **b**) of the wallrock basalt. The REE patterns of EM gabbronorites are also shown. See section "Interaction with basalt recorded by the East-Muren gabbroic dike" for more details

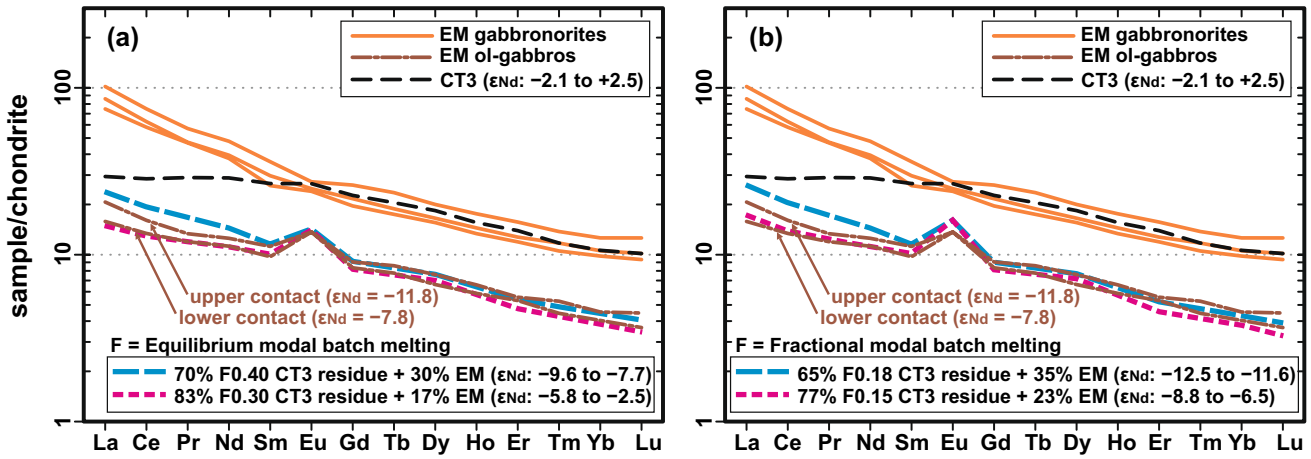

Fig. 9 Results of modeling of equilibrium batch melting (**a**) and fractional batch melting (**b**) of CT3 wallrock basalt (sample 6-MHR-94 with Nd isotopic variation of CT3 basalts) and mixing of such melt residues with infiltrating EM magma (sample 45-SKV-00) to simulate the formation of the EM contact zones shown in REE diagrams normalized to chondrite of McDonough and Sun (1995). The modal composition and partition coefficients of the partial melting model for the wallrock basalt as in Fig. 8. "F" denotes the degree of partial melting (equilibrium in **a** and fractional in **b**) of the wallrock basalt. The REE patterns of EM gabbronorites are also shown. See section "Interaction with basalt recorded by the East-Muren gabbroic dike" for more details

wallrock basalt in the models is 20% olivine, 30% clinopyroxene, and 50% plagioclase; such assemblage has been suggested to control the fractionation of the CT3 basalts with Mg# < 0.55 (Luttinen and Furnes 2000). Additional details on the used partition coefficients are presented in the caption of Fig. 8. The infiltrating EM magma was estimated to correspond to the EM middle zone gabbronorite composition (sample 45-SKV-00).

Our modeling of the hornfelses shows that their REE patterns can be explained reasonably well by the hornfelses being residues of 6−9% equilibrium batch partial melting of CT3 basalt (Fig. 8a). In contrast, fractional melting results in excessively depleted LREE compositions in the models compared to the hornfelses (Fig. 8b). In the best-fit models, higher degrees of partial melting are suggested for the upper contact hornfels, which is also compatible with its relatively higher MgO and Ni contents (Fig. 3).

The geochemical evidence of partial melting is supported by textural evidence from the basalt hornfelses, such as the resorbed texture of the clinopyroxene phenocrysts with small plagioclase embayments and high amounts of (residual) olivine and Fe–Ti oxides in the groundmass (Fig. 6c). Such or similar mineralogical changes have been described from partially melted mafic rocks elsewhere (e.g., Ferry et al. 1987; Brandriss et al. 1996; Leuthold et al. 2018).

To replicate the low REE concentrations but LREE-enriched patterns of the olivine gabbros in the contact zones, we increased the degree of partial melting of the wallrock basalt and infiltrated the residue with EM magma. Such hybrids with wallrock residues of 15−40% of equilibrium or fractional batch partial melting in a mixture with 17−35 wt.% of EM magma show striking similarity to the upper and lower contact zones, also in terms of ε_{Nd} (Fig. 9). Again, the best-fit models suggest higher degree of melting for the upper contact zone. Based on these models, we suggest that the EM contact zone "olivine gabbros" did not crystallize directly from the EM parental magma, but represent hybrids of EM magmas with residual wallrock basalts that had been depleted by prior removal of partial melt. The pyroxene-rich stripes and leucocratic intercalations reported by Vuori and Luttinen (2003) from the contact zone could, thus, represent the residual wallrock basalt and the infiltrated EM magma, respectively. Although both melting models (equilibrium and fractional) provide reasonable fits for the trace element patterns of the EM contact zones, differences arise in terms of Nd isotopes (Fig. 9): Nd isotopic compositions of the residue–magma mixtures in the fractional melting models are more similar to those measured from the contact zones.

The presented models suggest that whereas the low-degree partial melts were retained in the distal wallrock basalt hornfelses before being extracted (equilibrium melting), the proximal contact zones experienced more continuous melt depletion (fractional melting) before being infiltrated with EM magma. We emphasize that the presented degrees and processes of melting and the mixing ratios should not be taken as absolutes, however, since non-modal melting processes were likely involved as exemplified by the presence of orthopyroxene in some parts of the hornfels residue (Vuori and Luttinen 2003). In addition, the exact composition of the EM magma that reacted with the wallrock basalt residue cannot be as tightly constrained as presented in the models. Finally, we should note that the fate of the partial melts extracted from the wallrock basalts has not yet been discussed. Judging from the uniform ε_{Nd} of the EM middle zone (Fig. 3), they have not notably influenced the currently exposed rocks of the intrusion itself—at least in the present sampling scale. We suggest that magmas that were contaminated by the wallrock partial melts flowed upwards in the EM magma conduit before the contact zone was thermodynamically sealed for further contamination. The contaminated magmas were transported to shallower levels in the magma system and possibly erupted as basalts on the surface. This hypothesis is discussed in more detail later.

Interaction with basalt recorded by the West-Muren gabbroic dike

The WM gabbroic dike displays a general gradational geochemical change from the basal olivine gabbros of the main zone to the intermediate–felsic margin (Fig. 4). Coupling of chemical and Nd isotopic variations indicates progressive assimilation during the crystallization of the gabbroic dike. Positive correlation between the ε_{Nd} values and fractionation indexes (such as MgO and Ni; Fig. 4) suggests that the assimilated material had a relatively more radiogenic Nd isotopic composition than the parental magma.

Since major element data for a reasonable parental melt estimate and wallrock basalt are available (see below), we modeled the evolution of the WM magma system using the Magma Chamber Simulator (MCS; Bohrson et al. 2014) that models simultaneous crystallization and assimilation of magma + wallrock system in a thermodynamically consistent fashion. The main zone rocks of the WM gabbroic dike themselves are likely to be cumulates and are, thus, unsuitable to represent melt compositions. However, Luttinen et al. (2015) have reported compositions of other CT1 dikes that are fine-grained and do not show significant evidence of internal differentiation. We chose a low-ε_{Nd} CT1 dike sample AL/P5-98 from that study to represent the major and trace element composition of the parental melt: this sample is fairly primitive (MgO = 10.6 wt.%) and records Th/Ta, La/Sm, and initial ε_{Nd} similar to the WM main zone (Fig. 2). Note that this dike composition has, thus, experienced contamination by Archean crust (first stage of assimilation), which was modeled for the WM gabbroic dike previously. H_2O contents of the parental melt were constrained using H_2O/Ce of 600 (Heinonen et al. 2019) and the Nd isotopic composition of the parental melt was adjusted to conform to the most unradiogenic Nd isotopic composition analyzed from the WM main zone ($\varepsilon_{Nd} = -9.0$; sample 32-SKV-00). The AFC simulation was run at low pressure (100 MPa) and the preheated (800 °C) wallrock composition was that of the CT3 wallrock basalt 6-MHR-94 with 0.5 wt.% of H_2O that equals to the loss-on-ignition measured from the sample. After equilibration with the wallrock was reached, the remaining melt was further fractionated in a separate FC simulation. Trace element partition coefficients were adopted from the PELE software (Boudreau 1999; compilation by Jean Bedard); constant values were used since both parental magma and wallrock are basaltic and felsic compositions were not involved in the simulations.

All input and output for the MCS simulations are listed in Online Resource 2.

In the simulation, the reconstructed parental melt and initial basalt wallrock yielded a gabbroic mineral assemblage in the cumulate pile and a gabbronoritic wallrock restite, respectively, which is in accordance with the field observations. In the model, assimilation begins in basaltic magma after ~ 4% of crystallization (all percentages given relative to the mass of the parental melt). After ~ 32% of crystallization and ~ 12% of assimilation, the magma reached thermal equilibrium with the wallrock. At this stage the magma composition has initial ε_{Nd} of − 5.4, i.e., similar to that recorded in the intermediate–felsic margin (− 5.5). Further fractionation (~ 48%) of this magma results in a magma composition that has SiO_2 of 63 wt.%, which is within the range recorded in the intermediate–felsic margin (57–66 wt.% SiO_2). The incompatible trace element pattern of this modeled magma together with those of the parental melt, the basalt wallrock, and the margin rocks are illustrated in Fig. 10. Except for Ti, the model composition plots within or close to the field defined by the intermediate and felsic members of the margin, which show evidence of internal variation in the contents of apatite (in P), zircon (in Zr and Hf), oxides (in Ti), and/or amphibole (in Ti).

The presented simulation shows that an AFC + FC scenario involving a crystallizing basaltic magma partially melting a basaltic wallrock (+ xenoliths) is both thermodynamically and geochemically feasible for the origin of the chemical variability in the WM gabbroic dike. The rocks between the lowermost gabbroic sample and the intermediate–felsic margin crystallized and accumulated at some point along the evolutionary path of the residual magma(s). The model of emplacement will be discussed in more detail in the next section. It is important to note that because the MCS does not model the physical environment and magma flow through the conduit, the suggested degree of crystallization does not likely correspond to any absolute value and is not directly translatable to the areal extent of the intrusion at the current level of exposure.

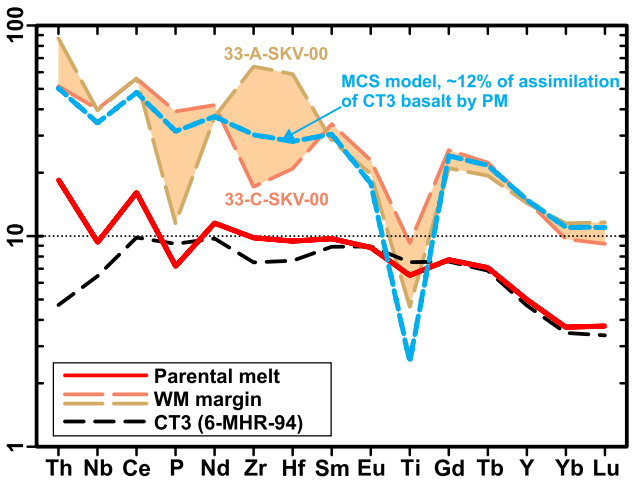

Fig. 10 Results of MCS modeling of assimilation of CT3 wallrock basalt by a hypothetical WM parental melt shown in incompatible trace element diagram normalized to primitive mantle of Sun and McDonough (1989). The samples from the WM intermediate–felsic margin are shown for comparison. See section "Interaction with basalt recorded by the West-Muren gabbroic dike" for more details

Schematic models for the differentiation and emplacement of the Muren gabbroic dikes

The Muren gabbroic dikes record different histories of magmatic evolution. Our preferred petrogenetic models are illustrated in Figs. 11 and 12 which represent the current orientation and level of exposure for the dikes.

According to EC-AFC modeling, the EM gabbroic dike records relatively higher degree of assimilation of Archean crust at depth (~ twice to that for WM; Fig. 7). This could also explain the abundant Ca-poor pyroxene in it (Fig. 6a), since assimilation of felsic TTG wallrock would increase silica activity in the melt which, in turn, would favor crystallization of orthopyroxene over olivine (see Grove and Juster 1989; Barnes et al. 2016; Heinonen et al. 2019; Mao et al. 2019). At shallow subvolcanic level, the ascending magma partially melted the wallrock basalts. The geochemical homogeneity of the dike interior suggests that the wallrock partial melts were either (1) transported away from the contact, (2) assimilated close to the dike margins not currently sampled, or (3) assimilated by earlier batches of EM magma that passed through. These options are not mutually exclusive. In any case, it is likely that the formation of the hybrid "olivine gabbro" in the contact zone sealed the contact from assimilation at some point of the evolution of the EM magma system (Fig. 11). This behavior is related to the magma dynamics, which will be discussed in the next section. Finally, EM middle zone lacks evidence of any accumulation or internal differentiation processes in the near vertical dike, although settling of crystals below the present level of exposure cannot be precluded.

In comparison, the WM gabbroic dike represents low-ε_{Nd} CT1 magmas less contaminated by the Archean crust compared to EM (Fig. 7), and also records in situ evidence of assimilation of wallrock basalts in the shallower crust (Fig. 10). Part of the assimilation may have taken place via the partial melting of entrained basalt xenoliths, which are abundantly found in the intrusion and could have been stoped from the roof of the subvertical conduit early during its emplacement. In addition to signs of assimilation, the WM main zone shows notable variations in major element concentrations (Fig. 4), which is evidence of internal crystal fractionation and accumulation processes. The Al_2O_3-rich roof zone is suggested to record flotation of plagioclase

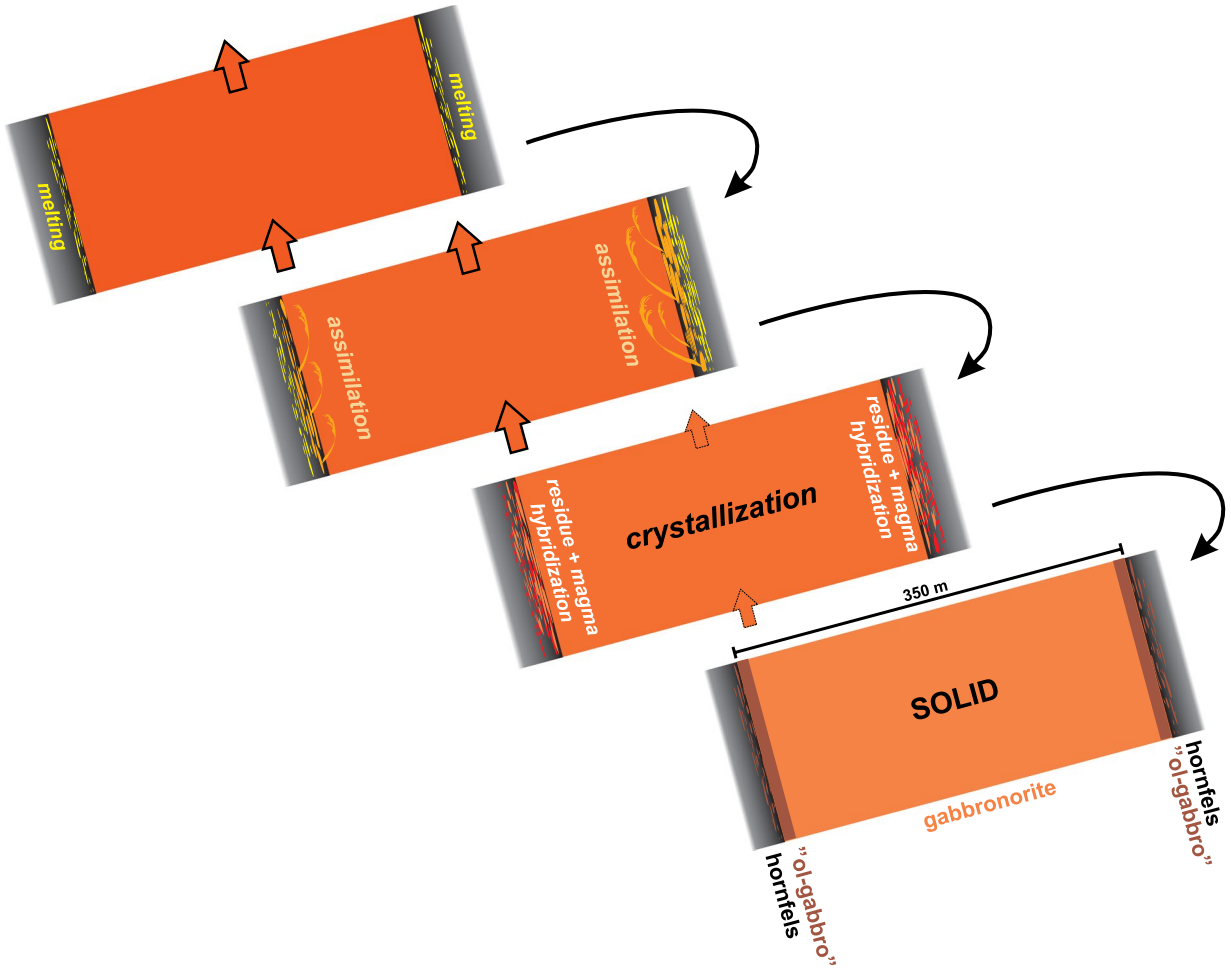

Fig. 11 Schematic model of magmatic evolution for the EM gabbroic dike illustrated in four snapshots of a vertical cross-section similar to the one shown in Fig. 1c. The black thin arrows of time connect the snapshots until the present situation, which is depicted by the right-most image. Filled arrows depict hypothetical magma flow. Individual crystals are not shown to preserve clarity. See section "Differentiation and emplacement of the Muren gabbroic dikes" for more details

close to the upper contact (Fig. 12); plagioclase flotation at an early stage is in accordance with the roof zone showing slightly more radiogenic Sr isotopic composition than the main zone sample 8-MHR-94 beneath it (see Online Resource 1).

Thermophysical considerations

The proclivity and extent of partial melting of wallrock depends very strongly on the transport history of the EM and WM magmas. One can imagine two limiting and contrasting transport dynamic regimes (e.g., Bruce 1989; Bruce and Huppert 1990; Fialko and Rubin 1999; Petcovic and Dufek 2005; Heinonen et al. 2019). For an intrusive body with negligible magma throughput (stagnant magma), the heat available for wallrock heating and possible partial fusion per unit time is directly proportional to the mass of the intrusive body, the temperature difference between wallrock and magma ($\Delta T = T_M - T_{WR}$), the magma–wallrock surface area, and the thermophysical properties of wallrock and magma (e.g., thermal conductivity, density, heat capacity). If hydrothermal convection is active, parameters such as the wallrock permeability and the transport and thermodynamic properties of the hydrothermal fluid are important as well (see discussion in Bohrson et al. 2014). A second limiting condition pertains to steady or quasi-steady sustained (weeks to months to years; White et al. 2006; Karlstrom et al. 2019) ascent of magma in a conduit. In a quasi-steady flow, the heat transfer from magma to wallrock is directly proportional to the flow rate and flow duration. The main factors are the pressure gradient driving magma flow, the conduit width and its vertical extent, and the temperature difference between wallrock and magma (Spera 1992). The last factor is closely related to the depth at which thermal interaction

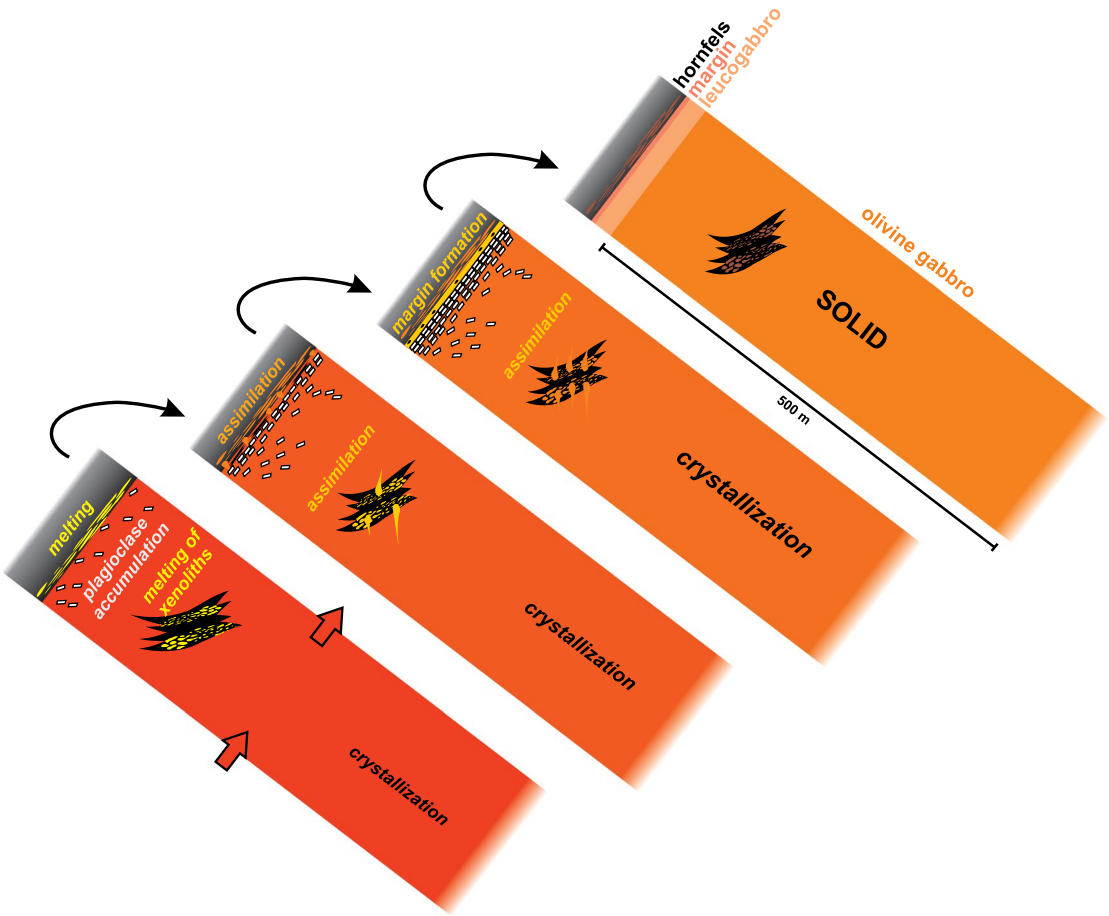

Fig. 12 Schematic model of magmatic evolution for the WM gabbroic dike illustrated in four snapshots of a vertical cross-section similar to the one shown in Fig. 1c. The black thin arrows of time connect the snapshots until the present situation, which is depicted by the rightmost image. Filled arrows depict hypothetical magma flow. Individual crystals, apart from accumulated plagioclase in the roof zone, are not shown to preserve clarity. See section "Differentiation and emplacement of the Muren gabbroic dikes" for more details

takes place. Here, we consider the relevant macroscopic balances of these two limiting cases. It is recognized that magma transport/storage scenarios involve elements of both scenarios to varying degree, perhaps even for a single episode of magma mobility. In the case of the EM and WM magma conduits, the sustained flow limit may be more pertinent to conditions at depth and the intrusive storage limit more relevant to the shallower crustal regime.

For magma storage as a tabular body of width (w), along strike length (l) and vertical extent (h), the lateral extent of the host partial melt region is thin, generally a very small fraction of the minimum dimension of the tabular intrusive body taken here as w. In conductive models, the temperature at the boundary between host wallrock and magma rapidly takes on the value of the average between the initial magma and far-field wallrock temperature. At shallow depths, this boundary temperature is subsolidus and melting will be suppressed in general except in a very narrow region of order meters or less. In contrast, at lower crustal depths where the ambient wallrock temperature is higher following the geotherm, partial melting extends significantly farther into wallrock, and therefore, approaches a larger fraction of w (see Heinonen et al. 2019). For an intrusive body, the volume (V), mass (m), and surface area (A) are, respectively: $V = whl$, $m = \rho_{\mathrm{M}} whl$, and $A = 2\,[hl + w\,(h+l)]$. The enthalpy (Q) available for heating and perhaps partial melting of wallrock is $Q = \rho_{\mathrm{M}} c_{\mathrm{p}}^{\mathrm{M}} whl\,\Delta T$, and this, together with the conductive heat flux ($q = k\,\Delta T/w$, where k is thermal conductivity) defines a timescale for conductive cooling and solidification, of the order $t_{\mathrm{c}} = Q/qA \approx \rho_{\mathrm{M}}\, c_{\mathrm{p}}^{\mathrm{M}} w^2/2k$. The thickness of the thermal aureole, therefore, scales as w and the region where the local wallrock temperature exceeds the wallrock solidus for a granitic bulk composition is about 0.05−0.1 times w based on conduction calculations (e.g., Carslaw and Jaeger 1959). Hence, in the case of the studied Muren gabbroic dikes, partial melting in the mid- to lower crust could have contaminated pristine

mantle-derived basaltic magma to the extent of about 3–6% as suggested from EC-AFC modeling.

For laminar flow in a rectangular conduit, the magma mass flow (kg/s) is $\dot{m} = (\Delta p^* l \rho_M w^3)/(12\,\eta h k)$, where Δp^* is the pressure driving magma ascent ($\Delta p^* = \Delta\rho_{excess} + \Delta\rho g h$; $\Delta\rho = \rho_{WR} - \rho_M$) and η is magma viscosity. For sustained (quasi-steady) flow appropriate for flood basaltic eruptions, lateral heat loss is balanced by vertical heat advection and viscous head loss is balanced by the pressure driving the flow. Elementary scaling of the energy and the vertical-component of the momentum equation leads to the scale relations $\rho_M c_p^M V w^2 \approx kh$ and $\Delta p^*/h \approx \eta V/w^2$, respectively. These scale relations express the balance between conductive lateral heat loss and advective heat transport and the balance between pressure and viscous forces relevant to flow in a tabular crack. The condition for significant partial melting in wallrock is that heat advection dominates over heat conduction or that the Péclet number (see Bejan 2004), defined in this case as $Pe = \rho_M c_p^M V w^2/kh$, exceeds unity (Bird et al. 2007). For conduits much deeper than wide (i.e., dikes), the velocity from the momentum equation scaling can be used to show that advective heat transport dominates over conductive heat transport ($Pe > 1$) for conduit widths greater than a few meters when the flow is sustained and other nominal values are used for magma and wallrock properties. This would lead to significant wallrock meltback, but the key limiting parameter here is the assumed sustained magma flow. Given the observed widths of the EM and WM dikes and the relatively restricted thermal effects noted for the EM dike, it seems unlikely that at any one time the whole of the conduit width was actively involved in upflow. The mass flow (kg/s) upwards in a single active conduit with w of 100 m from the Hagen–Poiseuille equation cited above ($\dot{m}$) gives a volumetric discharge of ~ 0.1 km^3/s, an unrealistically high value. Even in the case of smaller discharge rates, the anomalously large size of the Muren conduits was nevertheless likely to promote wallrock meltback also in the shallower crust.

In summary, although it is impossible to know with sufficient certainty the whole geometry and active flow conditions (including temporal variations in them) of the EM and WM magma conduits, scaling suggests that contamination with Archean partial melts at depth followed by a second phase of contamination at shallow depths is not only energetically and dynamically possible but indeed likely in their case. The width of the WM gabbroic dike is ≥ 1.5 times that of the EM gabbroic dike at the current level of exposure—assuming otherwise uniform or similar values for the other thermophysical variables listed above, this is compatible with the WM gabbroic dike showing clearer evidence of wallrock basalt assimilation. On the other hand, entrainment of wallrock xenoliths in WM magma also likely had influence in its capability to assimilate basalt more efficiently. In comparison to these exceptionally large conduits, for considerably thinner ($w < 10$ m) dikes that are dominant in the study area, shallow-level assimilation is nevertheless not as likely (see an example for w of 1.5 m in Heinonen et al. 2019).

Wider implications of the presented models

When magmas pass through the continental crust, they interact with a wide variety of rock types in different parts of the magma transport system. The presented MCS modeling lends support to the idea that basaltic magmas are able to assimilate other mafic rocks, potentially in significant quantities (see also Borisova et al. 2017; Potter et al. 2018; cf. Tegner et al. 2005). The thermodynamic explanation for this process is the marked gap between the liquidus and solidus temperatures of basalts and the significant release of latent heat during crystallization. The solidus temperature of a mafic wallrock is further lowered and melt productivity increased by increase in the degree of hydrothermal alteration (see, e.g., Ellis and Thompson 1986; Clemens and Vielzeuf 1987; France et al. 2010).

Our study further illustrates a confounding aspect of multi-stage assimilation of wallrock when one of the contaminants is geochemically similar to the parental magmas of the studied system. In the case of a lava suite, it would be difficult to identify that a mass exchange had taken place even if geochemical data on the phenocryst phases were available. Most likely, the compositions most severely affected by the wallrock basalt component would be regarded to represent the least contaminated samples of the magma system. For example, if we would have analyzed only lavas having isotopic compositions akin to those recorded by the most evolved mafic portions of the WM gabbroic dike, we would probably have missed the assimilation of wallrock basalts and interpreted the samples showing the highest ε_{Nd} to be the least contaminated. We were able to recognize the assimilation of wallrock basalt because of the well-exposed cross-sections of the gabbroic dike and because the wallrock basalts are isotopically drastically different from the intruded low-ε_{Nd} CT1 magmas.

In mafic LIPs, magmatic cannibalism as described here would be expected to lead to homogenization of geochemical variations derived from mantle heterogeneity and contamination with silicic crust and, obviously, hamper the tracing of mantle-derived signatures. Although the pronounced geochemical heterogeneity of the flood basalts in our study area (Fig. 2) and worldwide suggests that a large part of the magma heterogeneities persist, for some high-volume magmatic phases the internal homogenization processes may be notable. For example, the most

voluminous phase of the Karoo LIP magmatism produced the extensive "North Karoo" low-Ti basalts that show rather uniform geochemical compositions (see. e.g., Luttinen 2018). Whether this geochemical homogeneity stems from homogeneous sources or LIP cannibalism remains to be studied. Examples of mafic intrusions within mafic wallrocks are known from several LIPs worldwide (e.g., Habekost and Wilson 1989; Miller and Ripley 1996; Shellnutt 2014). For example, the Skaergaard layered intrusion in eastern Greenland has traditionally been considered to represent a largely closed-system event (e.g., Nielsen 2004), regardless of some indications of minor assimilation of Archean gneisses (e.g., Stewart and DePaolo 1990; McBirney and Creaser 2003; Hagen-Peter et al. 2019). The roof of the intrusion consists of petrogenetically associated flood basalts that have been heavily altered by hydrothermal fluids (Taylor and Forester 1979). The isotopic similarity between the Skaergaard intrusion and the basalts of the area (McBirney and Creaser 2003) imply that it may be difficult to evaluate the role of wallrock assimilation in this case.

Finally, it should be emphasized that most voluminous part of LIP igneous activity takes place in the mantle and in the lower crust (e.g., White and McKenzie 1989; Coffin and Eldholm 1994; Bryan and Ernst 2008; Rohrman 2013; Ernst et al. 2019). Lower crust is predominantly mafic and also contains intrusions and cumulates that are relatively warm and were left behind by earlier LIP magma pulses (Rudnick et al. 1986). Potential cannibalization of such formations by large quantities of primitive and hot mantle-derived magmas like recently suggested for oceanic Kerguelen LIP (e.g., Borisova et al. 2017) would multiply the effects of assimilation observed in the upper crustal environment of this study. Such processes may be important in the formation of, for example, massif-type anorthosites, the origin of which has been a longstanding petrological issue (e.g., Duchesne et al. 1999; Ashwal and Bybee 2017; He et al. 2019), and the generation of the "ghost plagioclase" signature observed in some OIBs and originally suggested to reflect recycled crust in the mantle source (Sobolev et al. 2000; cf. Peterson et al. 2014). We therefore encourage future thermodynamic and geochemical modeling of cannibalization and assimilation of mafic crust in magmatic systems.

Conclusions

Two moderately dipping gabbroic dikes (East- and West-Muren; EM and WM) that crosscut flood basalts belonging to the ~ 180 Ma Karoo LIP in Vestfjella, western Dronning Maud Land, Antarctica, show peculiar geochemical characteristics: their initial ε_{Nd} values increase towards the contact with the wallrock basalts. The petrogenesis of these dikes and their wallrock aureoles were modeled using partial melting equations and energy-constrained assimilation−fractional crystallization modeling tools. The incompatible element ratios and Nd isotopic compositions of both gabbroic dikes suggest that the parental magmas first assimilated Archean TTGs at deeper crustal levels. For the ~ 350 m wide EM gabbroic dike, the increase in ε_{Nd} is observed in the contact zones that have previously been mapped as olivine gabbros. Our modeling of partial melting and mixing show that these zones were formed by partial melting of the isotopically more depleted wallrock basalts and hybridization of these melt residues with the EM magmas. In the case of the ≥ 500-m-wide WM gabbroic dike, the intrusion records more continuous increase in ε_{Nd} towards the roof contact, which is compatible with notable assimilation of the wallrock basalts by the crystallizing magma. The examples presented here show that basaltic magmas are able to melt basalts in potentially significant quantities. Such processes have potential to cause (1) oversimplifications in interpretations of magmatic differentiation, (2) homogenization of geochemical signatures of LIP magmas, and (3) notable hybrid magma generation, especially in the lower crust.

Supplementary Information The online version contains supplementary material available at https://doi.org/10.1007/s00410-021-01777-6.

Acknowledgements We thank the reviewers (Kurt S. Panter and an anonymous reviewer) for the encouraging and constructive comments and editor Mark Ghiorso for professional handling of the manuscript. We are grateful for the various FINNARP research expeditions that enabled the collection of the studied samples from these very remote areas; Mika Räisänen is especially thanked for providing many of the samples, which he studied in relation to his MSc Thesis. The staff of the Peter Hooper GeoAnalytical Lab of the Washington State University is thanked for the major element and trace element analyses and for the help and guidance in sample preparation on site. We are also very grateful to John Lassiter and the staff at the Isotope Geochemistry labs of the Department of Geological Sciences, University of Texas at Austin, for providing swift and high-precision Nd isotopic analyses. J. Heinonen wants to thank Melissa Scruggs for the feedback and suggestions she provided for this study in its infant stages. The research has highly benefited from the funding provided by the Academy of Finland Grants 295129 and 305663. W. Bohrson thanks the National Science Foundation for supporting development of the modeling tools used in this study.

Funding Open access funding provided by University of Helsinki including Helsinki University Central Hospital.

References

Ashwal LD, Bybee GM (2017) Crustal evolution and the temporality of anorthosites. Earth-Sci Rev 173:307–330. https://doi.org/10.1016/j.earscirev.2017.09.002

Baker JA, Thirlwall MF, Menzies MA (1996) Sr-Nd-Pb isotopic and trace element evidence for crustal contamination of plume-derived flood basalts: oligocene flood volcanism in western Yemen. Geochim Cosmochim Acta 60:2559–2581. https://doi.org/10.1016/0016-7037(96)00105-6

Barnes SJ, Mole DR, Le Vaillant M, Campbell MJ, Verrall MR, Roberts MP, Evans NJ (2016) Poikilitic textures, heteradcumulates and zoned orthopyroxenes in the Ntaka Ultramafic Complex, Tanzania: implications for crystallization mechanisms of oikocrysts. J Petrology 57:1171–1198. https://doi.org/10.1093/petrology/egw036

Bejan A (2004) Convection heat transfer, 3rd edn. John Wiley & Sons, New York, United States, p 694

Bird RB, Stewart WE, Lightfoot EN (2007) Transport phenomena, 2nd edn. John Wiley & Sons, New York, United States, p 928

Bohrson WA, Spera FJ, Ghiorso MS, Brown GA, Creamer JB, Mayfield A (2014) Thermodynamic model for energy-constrained open-system evolution of crustal magma bodies undergoing simultaneous recharge, assimilation and crystallization: the magma chamber simulator. J Petrol 55:1685–1717. https://doi.org/10.1093/petrology/egu036

Borisova AY, Bohrson WA, Grégoire M (2017) Origin of primitive ocean island basalts by crustal gabbro assimilation and multiple recharge of plume-derived melts. Geochem Geophys Geosyst 18:2701–2716. https://doi.org/10.1002/2017GC006986

Boudreau AE (1999) PELE—a version of the MELTS software program for the PC platform. Comput Geosci 25:201–203. https://doi.org/10.1016/s0098-3004(98)00117-4

Brandon AD, Hooper PR, Goles GG, Lambert RSJ (1993) Evaluating crustal contamination in continental basalts: the isotopic composition of the Picture Gorge Basalt of the Columbia River basalt group. Contrib Miner Petrol 114:452–464. https://doi.org/10.1007/BF00321750

Brandriss ME, Bird DK, O'Neil JR, Cullers RL (1996) Dehydration, partial melting, and assimilation of metabasaltic xenoliths in gabbros of the Kap Edvard Holm complex, East Greenland. Am J Sci 296:333–393. https://doi.org/10.2475/ajs.296.4.333

Bruce PM (1989) Thermal Convection within the Earth's Crust. Ph.D. Thesis, University of Cambridge, United Kingdom, p 169

Bruce PM, Huppert HE (1990) Solidification and melting along dykes by the laminar flow of basaltic magma. In: Ryan MP (ed) Magma transport and storage. Wiley, New York (NY), United States, pp 87–101

Bryan SE, Ernst RE (2008) Revised definition of large igneous provinces (LIPs). Earth-Sci Rev 86:175–202. https://doi.org/10.1016/j.earscirev.2007.08.008

Carslaw HS, Jaeger JC (1959) Conduction of heat in solids. Oxford University Press, Oxford, United Kingdom, p 510

Clemens JD, Vielzeuf D (1987) Constraints on melting and magma production in the crust. Earth Planet Sci Lett 86:287–306. https://doi.org/10.1016/0012-821X(87)90227-5

Coffin MF, Eldholm O (1994) Large igneous provinces: Crustal structure, dimensions, and external consequences. Rev Geophys 32:1–36. https://doi.org/10.1029/93RG02508

Corner B (1994) Geological evolution of western Dronning Maud Land within a Gondwana framework: geophysics subprogramme. Final project report to SACAR. Department of Geophysics, Witwatersrand University, South Africa, p 21

Cox KG (1980) A model for flood basalt vulcanism. J Petrol 21:629–650. https://doi.org/10.1093/petrology/21.4.629

Duchesne JC, Liégeois JP, Vander Auwera J, Longhi J (1999) The crustal tongue melting model and the origin of massive anorthosites. Terra Nova 11:100–105. https://doi.org/10.1046/j.1365-3121.1999.00232.x

Ellis DJ, Thompson AB (1986) Subsolidus and Partial melting reactions in the quartz-excess CaO + MgO + Al_2O_3 + SiO_2 + H_2O system under water-excess and water-deficient conditions to 10 kb: some implications for the origin of peraluminous melts from mafic rocks. J Petrology 27:91–121. https://doi.org/10.1093/petrology/27.1.91

Ernst RE (2007) Mafic-ultramafic large igneous provinces (LIPs): importance of the pre-Mesozoic record. Episodes 30:108–114. https://doi.org/10.18814/epiiugs/2007/v30i2/005

Ernst RE, Liikane DA, Jowitt SM, Buchan KL, Blanchard JA (2019) A new plumbing system framework for mantle plume-related continental large igneous provinces and their mafic-ultramafic intrusions. J Volcanol Geotherm Res 384:75–84. https://doi.org/10.1016/j.jvolgeores.2019.07.007

Ferry JM, Mutti LJ, Zuccala GJ (1987) Contact metamorphism/hydrothermal alteration of Tertiary basalts from the Isle of Skye, northwest Scotland. Contrib Miner Petrol 95:166–181. https://doi.org/10.1007/BF00381266

Fialko YA, Rubin AM (1999) Thermal and mechanical aspects of magma emplacement in giant dike swarms. J Geophys Res 104:23033–23049. https://doi.org/10.1029/1999JB900213

France L, Koepke J, Ildefonse B, Cichy SB, Deschamps F (2010) Hydrous partial melting in the sheeted dike complex at fast spreading ridges: experimental and natural observations. Contrib Miner Petrol 160:683–704. https://doi.org/10.1007/s00410-010-0502-6

Grosch EG, Bisnath A, Frimmel HE, Board WS (2007) Geochemistry and tectonic setting of mafic rocks in western Dronning Maud Land, East Antarctica: implications for the geodynamic evolution of the Proterozoic Maud Belt. J Geol Soc 164:465–475. https://doi.org/10.1144/0016-76492005-152

Grosch EG, Frimmel HE, Abu-Alam T, Košler J (2015) Metamorphic and age constraints on crustal reworking in the western H.U. Sverdrupfjella: implications for the evolution of western Dronning Maud land. Antarctica J Geol Soc 172:499–518. https://doi.org/10.1144/jgs2014-090

Grove TL, Juster TC (1989) Experimental investigations of low-Ca pyroxene stability and olivine-pyroxene-liquid equilibria at 1 atm in natural basaltic and andesitic liquids. Contrib Miner Petrol 103:287–305. https://doi.org/10.1007/BF00402916

Habekost EM, Wilson JR (1989) Raft-like metabasaltic inclusions in the fongen-hyllingen layered intrusive complex, Norway, and their implications for magma chamber evolution. J Petrology 30:1415–1441. https://doi.org/10.1093/petrology/30.6.1415

Hagen-Peter G, Tegner C, Lesher CE (2019) Strontium isotope systematics for plagioclase of the Skaergaard intrusion (East Greenland): a window to crustal assimilation, differentiation, and magma dynamics. Geology 47:313–316. https://doi.org/10.1130/G45639.1

Hansen H, Nielsen TFD (1999) Crustal contamination in Palaeogene East Greenland flood basalts: plumbing system evolution during continental rifting. Chem Geol 157:89–118. https://doi.org/10.1016/S0009-2541(98)00196-X

Hayes B, Bédard JH, Hryciuk M, Wing B, Nabelek P, MacDonald WD, Lissenberg CJ (2015) Sulfide immiscibility induced by wall-rock assimilation in a fault-guided Basaltic feeder system, Franklin large igneous province, Victoria Island (Arctic Canada).

Economicgeology 110:1697–1717. https://doi.org/10.2113/econgeo.110.7.1697
He H, Song X, Zhai M, Yu S, Du Z (2019) Lower crustal contribution to the magma formation of the Damiao massif-type anorthosite, North China Craton: evidence from zircon Hf-O isotopes. Precambr Res 332:105396. https://doi.org/10.1016/j.precamres.2019.105396
Heinonen JS, Carlson RW, Luttinen AV (2010) Isotopic (Sr, Nd, Pb, and Os) composition of highly magnesian dikes of Vestfjella, western Dronning Maud land, Antarctica: a key to the origins of the Jurassic Karoo large igneous province? Chem Geol 277:227–244. https://doi.org/10.1016/j.chemgeo.2010.08.004
Heinonen JS, Luttinen AV, Bohrson WA (2016) Enriched continental flood basalts from depleted mantle melts: modeling the lithospheric contamination of Karoo lavas from Antarctica. Contrib Miner Petrol 171:9. https://doi.org/10.1007/s00410-015-1214-8
Heinonen JS, Luttinen AV, Whitehouse MJ (2018) Enrichment of 18O in the mantle sources of the Antarctic portion of the Karoo large igneous province. Contrib Miner Petrol 173:21. https://doi.org/10.1007/s00410-018-1447-4
Heinonen JS, Luttinen AV, Spera FJ, Bohrson WA (2019) Deep open storage and shallow closed transport system for a continental flood basalt sequence revealed with magma chamber simulator. Contrib Miner Petrol 174:87. https://doi.org/10.1007/s00410-019-1624-0
Hersum TG, Marsh BD, Simon AC (2007) Contact partial melting of granitic country rock, melt segregation, and re-injection as dikes into ferrar dolerite sills, McMurdo Dry Valleys, Antarctica. J Petrol 48:2125–2148. https://doi.org/10.1093/petrology/egm054
Jacobs J, Fanning CM, Bauer W (2003) Timing of Grenville-age vs. Pan-African medium- to high grade metamorphism in western Dronning Maud land (East Antarctica) and significance for correlations in Rodinia and Gondwana. Precambrian Res 125:1–20. https://doi.org/10.1016/S0301-9268(03)00048-2
Jacobs J, Pisarevsky S, Thomas RJ, Becker T (2008) The Kalahari Craton during the assembly and dispersal of Rodinia. Precambrian Res 160:142–158. https://doi.org/10.1016/j.precamres.2007.04.022
Jacobs J, Elburg M, Läufer A, Kleinhanns IC, Henjes-Kunst F, Estrada S, Ruppel AS, Damaske D, Montero P, Bea F (2015) Two distinct late mesoproterozoic/early neoproterozoic basement provinces in central/eastern Dronning Maud land, East Antarctica: the missing link, 15–21°E. Precambr Res 265:249–272. https://doi.org/10.1016/j.precamres.2015.05.003
Johnson DM, Hooper PR, Conrey RM (1999) XRF analysis of rocks and minerals for major and trace elements on a single low dilution Li-tetraborate fused bead. Adv X-Ray Anal 41:843–867
Johnson TE, Gibson RL, Brown M, Buick IS, Cartwright I (2003) Partial melting of metapelitic rocks beneath the Bushveld Complex, South Africa. J Petrol 44:789–813. https://doi.org/10.1093/petrology/44.5.789
Karlstrom L, Murray KE, Reiners PW (2019) Bayesian markov-chain monte carlo inversion of low-temperature thermochronology around two 8–10 m wide Columbia river flood basalt dikes. Front Earth Sci 7:90. https://doi.org/10.3389/feart.2019.00090
Knaack C, Cornelius SB, Hooper PR (1994) Trace element analyses of rocks and minerals by ICP-MS. Washington State University, GeoAnalytical Lab
Kreissig K, Naegler TF, Kramers JD, van Reenen DD, Smit CA (2000) An isotopic and geochemical study of the northern Kaapvaal Craton and the Southern Marginal zone of the Limpopo belt: are they juxtaposed terranes? Lithos 50:1–25. https://doi.org/10.1016/S0024-4937(99)00037-7
LeCheminant AN, Heaman LM (1989) Mackenzie igneous events, Canada: middle Proterozoic hotspot magmatism associated with ocean opening. Earth Planet Sci Lett 96:38–48. https://doi.org/10.1016/0012-821X(89)90122-2
Leuthold J, Lissenberg CJ, O'Driscoll B, Karakas O, Falloon T, Klimentyeva DN, Ulmer P (2018) Partial melting of lower oceanic crust gabbro: constraints from poikilitic clinopyroxene primocrysts. Front Earth Sci 6:15
Lightfoot PC, Naldrett AJ (1989) Assimilation and crystallization in basic magma chambers: trace-element and Nd-isotopic variations in the Kerns sill, Nipissing diabase province, Ontario. Can J Earth Sci 26:737–754. https://doi.org/10.1139/e89-061
Luttinen AV (2018) Bilateral geochemical asymmetry in the Karoo large igneous province. Sci Rep 8:5223. https://doi.org/10.1038/s41598-018-23661-3
Luttinen AV, Furnes H (2000) Flood basalts of Vestfjella: Jurassic magmatism across an Archaean-Proterozoic lithospheric boundary in Dronning Maud land, Antarctica. J Petrol 41:1271–1305. https://doi.org/10.1093/petrology/41.8.1271
Luttinen AV, Siivola JU (1997) Geochemical characteristics of Mesozoic lavas and dikes from Vestfjella, Dronning Maud Land: recognition of three distinct chemical types. In: Ricci CA (ed) The Antarctic region: geological evolution and processes, vol 7. Terra Antarctica Publications. Siena, Italy, pp 495–503
Luttinen A, Vuori S (2006) Geochemical correlations between Jurassic gabbros and basaltic rocks in Vestfjella, Dronning Maud Land, Antarctica. In: Hanski E, Mertanen S, Rämö T, Vuollo J (eds) Mafic Dykes – time markers of crustal evolution. Taylor & Francis Group, London, pp 201–212
Luttinen AV, Rämö OT, Huhma H (1998) Neodymium and strontium isotopic and trace element composition of a Mesozoic CFB suite from Dronning Maud land, Antarctica: implications for lithosphere and asthenosphere contributions to Karoo magmatism. Geochim Cosmochim Acta 62:2701–2714. https://doi.org/10.1016/S0016-7037(98)00184-7
Luttinen AV, Heinonen JS, Kurhila M, Jourdan F, Mänttäri I, Vuori SK, Huhma H (2015) Depleted mantle-sourced CFB magmatism in the Jurassic Africa-Antarctica rift: petrology and $^{40}Ar/^{39}Ar$ and U/Pb chronology of the Vestfjella Dyke swarm, Dronning Maud land, Antarctica. J Petrol 56:919–952. https://doi.org/10.1093/petrology/egv022
Mao Y, Barnes SJ, Qin K, Tang D, Martin L, Su B, Evans NJ (2019) Rapid orthopyroxene growth induced by silica assimilation: constraints from sector-zoned orthopyroxene, olivine oxygen isotopes and trace element variations in the Huangshanxi Niâ€"Cu deposit, Northwest China. Contrib Miner Petrol 174:33. https://doi.org/10.1007/s00410-019-1574-6
Marschall HR, Hawkesworth CJ, Storey CD, Dhuime B, Leat PT, Meyer H, Tamm-Buckle S (2010) The Annandagstoppane granite, East Antarctica: evidence for archaean intracrustal recycling in the Kaapvaal-Grunehogna craton from zircon O and Hf isotopes. J Petrol 51:2277–2301. https://doi.org/10.1093/petrology/egq057
McBirney AR, Creaser RA (2003) The Skaergaard layered series, part VII: Sr and Nd isotopes. J Petrology 44:757–771. https://doi.org/10.1093/petrology/44.4.757
McDonough WF, Sun SS (1995) The composition of the earth. Chem Geol 120:223–253. https://doi.org/10.1016/0009-2541(94)00140-4
McLoughlin S, Larsson K, Lindström S (2005) Permian plant macrofossils from Fossilryggen, Vestfjella. Dronning Maud Land Antarct Sci 17:73. https://doi.org/10.1017/S0954102005002464
Miller JD, Ripley EM (1996) Layered intrusions of the Duluth Complex, Minnesota, USA. Developments in Petrology 15:257–301. https://doi.org/10.1016/S0167-2894(96)80010-8
Moyes AB, Krynauw JR, Barton JM Jr (1995) The age of the Ritscherflya Supergroup and Borgmassivet intrusions, Dronning Maud land, Antarctica. Antarct Sci 7:87–97. https://doi.org/10.1017/S0954102095000125

Neumann E, Svensen H, Galerne CY, Planke S (2011) Multistage evolution of dolerites in the Karoo large igneous province, Central South Africa. J Petrol 52:959–984. https://doi.org/10.1093/petrology/egr011

Nielsen TFD (2004) The shape and volume of the Skaergaard intrusion, Greenland: implications for mass balance and bulk composition. J Petrology 45:507–530. https://doi.org/10.1093/petrology/egg092

Petcovic HL, Dufek JD (2005) Modeling magma flow and cooling in dikes: implications for emplacement of Columbia River flood basalts. J Geophys Res. https://doi.org/10.1029/2004jb003432

Peterson ME, Saal AE, Nakamura E, Kitagawa H, Kurz MD, Koleszar AM (2014) Origin of the 'Ghost Plagioclase' signature in Galapagos melt inclusions: new evidence from Pb isotopes. J Petrol 55:2193–2216. https://doi.org/10.1093/petrology/egu054

Potter KE, Shervais JW, Christiansen EH, Vetter SK (2018) Evidence for cyclical fractional crystallization, recharge, and assimilation in basalts of the Kimama drill core, Central Snake River plain, Idaho: 5.5 million years of petrogenesis in a mid-crustal sill complex. Front Earth Sci 6:10

Riley TR, Millar IL (2014) Geochemistry of the 1100 Ma intrusive rocks from the Ahlmannryggen region, Dronning Maud land, Antarctica. Antarct Sci 26:389–399. https://doi.org/10.1017/S0954102013000916

Rohrman M (2013) Intrusive large igneous provinces below sedimentary basins: an example from the Exmouth plateau (NW Australia). J Geophys Res Solid Earth 118:4477–4487. https://doi.org/10.1002/jgrb.50298

Romu KRI (2019) Origin of the concealed continental crust of Vestfjella, western Dronning Maud land. Evidence from xenoliths hosted by Jurassic lamproites, Antarctica

Rudnick RL, McDonough WF, McCulloch MT, Taylor SR (1986) Lower crustal xenoliths from Queensland, Australia: evidence for deep crustal assimilation and fractionation of continental basalts. Geochim Cosmochim Acta 50:1099–1115. https://doi.org/10.1016/0016-7037(86)90391-1

Schnetzler CC, Philpotts JA (1970) Partition coefficients of rare-earth elements between igneous matrix material and rock-forming mineral phenocrysts—II. Geochim Cosmochim Acta 34:331–340. https://doi.org/10.1016/0016-7037(70)90110-9

Shellnutt JG (2014) The Emeishan large igneous province: a synthesis. Geosci Front 5:369–394. https://doi.org/10.1016/j.gsf.2013.07.003

Sobolev AV, Hofmann AW, Nikogosian IK (2000) Recycled oceanic crust observed in "ghost plagioclase" within the source of Mauna Loa lavas. Nature 404:986–990

Spera FJ (1992) Lunar magma transport phenomena. Geochim Cosmochim Acta 56:2253–2265. https://doi.org/10.1016/0016-7037(92)90187-N

Spera FJ, Bohrson WA (2001) Energy-constrained open-system magmatic processes I: general model and energy-constrained assimilation and fractional crystallization (EC-AFC) formulation. J Petrol 42:999–1018. https://doi.org/10.1093/petrology/42.5.999

Stewart BW, DePaolo DJ (1990) Isotopic studies of processes in mafic magma chambers: II. The Skaergaard intrusion, East Greenland. Contrib Miner Petrol 104:125–141. https://doi.org/10.1007/BF00306438

Sun SS, McDonough WF (1989) Chemical and isotopic systematics of oceanic basalts: Implications for mantle composition and processes. In: Saunders AD, Norry MJ (eds) Magmatism in the ocean basins, vol 42. Geological Society Special Publications, United Kingdom (GBR), pp 313–345. https://doi.org/10.1144/GSL.SP.1989.042.01.19

Taylor HPj, Forester RW (1979) An oxygen and hydrogen isotope study of the Skaergaard intrusion and its country rocks: a description of a 55 M.Y. Old fossil hydrothermal system*. J Petrology 20:355–419. https://doi.org/10.1093/petrology/20.3.355

Tegner C, Wilson JR, Robins B (2005) Crustal assimilation in basalt and jotunite: constraints from layered intrusions. Lithos 83:299–316. https://doi.org/10.1016/j.lithos.2005.03.007

Turunen ST, Luttinen AV, Heinonen JS, Jamal DL (2019) Luenha picrites, Central Mozambique—messengers from a mantle plume source of Karoo continental flood basalts? Lithos 346–347:105152. https://doi.org/10.1016/j.lithos.2019.105152

Vanderkluysen L, Mahoney JJ, Hooper PR, Sheth HC, Ray R (2011) The feeder system of the Deccan Traps (India): insights from dike geochemistry. J Petrol 52:315–343. https://doi.org/10.1093/petrology/egq082

Vuori SK (2004) Petrogenesis of the Jurassic gabbroic intrusions of Vestfjella, Dronning Maud Land, Antarctica. PhD thesis, University of Helsinki, Helsinki, Finland p 25.

Vuori SK, Luttinen AV (2003) The Jurassic gabbroic intrusion of Utpostane and Muren: insights into Karoo-related plutonism in Dronning Maud land, Antarctica. Antarct Sci 15:283–301. https://doi.org/10.1017/S0954102003001287

White R, McKenzie D (1989) Magmatism at rift zones: the generation of volcanic continental margins and flood basalts. J Geophys Res 94:7685–7729. https://doi.org/10.1029/JB094iB06p07685

White SM, Crisp JA, Spera FJ (2006) Long-term volumetric eruption rates and magma budgets. Geochem Geophys Geosyst. https://doi.org/10.1029/2005GC001002

Wingate MTD, Pirajno F, Morris PA (2004) Warakurna large igneous province: a new Mesoproterozoic large igneous province in west-central Australia. Geology 32:105–108. https://doi.org/10.1130/G20171.1

Wolmarans LG, Kent KE (1982) Geological investigations in western Dronning Maud land, Antarctica—a synthesis. S Afr J Antarc Res Suppl 2:93

Yallup C, Edmonds M, Turchyn AV (2013) Sulfur degassing due to contact metamorphism during flood basalt eruptions. Geochim Cosmochim Acta 120:263–279. https://doi.org/10.1016/j.gca.2013.06.025

Authors and Affiliations

Jussi S. Heinonen[1,2] · Arto V. Luttinen[3] · Frank J. Spera[4] · Saku K. Vuori[5] · Wendy A. Bohrson[2,6]

Arto V. Luttinen
arto.luttinen@helsinki.fi

Frank J. Spera
spera@geol.ucsb.edu

Saku K. Vuori
saku.vuori@gtk.fi

Wendy A. Bohrson
bohrson@mines.edu

[1] Department of Geosciences and Geography, University of Helsinki, P.O. Box 64, 00014 Helsinki, Finland

[2] Department of Geological Sciences, Central Washington University, 400 E University Way, Ellensburg, WA 98926, USA

[3] Finnish Museum of Natural History, University of Helsinki, P.O. Box 44, 00014 Helsinki, Finland

[4] Department of Earth Science and Earth Research Institute, University of California Santa Barbara, Lagoon Rd, Santa Barbara, CA 93106, USA

[5] Geological Survey of Finland, P.O. Box 96, 02151 Espoo, Finland

[6] Department of Geology and Geological Engineering, Colorado School of Mines, 1516 Illinois St., Golden, CO 80401, USA